Journal of Sound and Vibration 617 (2025) 119319

Contents lists available at ScienceDirect

Journal of Sound and Vibration

journal homepage: www.elsevier.com/locate/jsvi

Tuned inerter viscoelastic liquid column dampers

Sudip Chowdhury [a,*], Rama Debbarma [b], Sondipon Adhikari [a]

[a] James Watt School of Engineering, The University of Glasgow, Glasgow, Scotland, United Kingdom
[b] Civil Engineering Department, National Institute of Technology Agartala, Agartala, Tripura, India

ARTICLE INFO

Keywords:
Tuned inerter viscoelastic liquid column damper (TIVLCD)
Tuned liquid column damper (TLCD)
Tuned liquid column damper with inertia (TLCDI)
Viscoelastic damping
H_∞ optimisation

ABSTRACT

Structural vibration control remains a major challenge in engineering, particularly for buildings exposed to dynamic excitations. While conventional Tuned Liquid Column Dampers (TLCDs) and inerter-based TLCDs offer passive damping solutions, they are limited in simultaneously optimising inertial and damping effects. This study proposes Tuned Inerter Viscoelastic Liquid Column Dampers (TIVLCDs), a novel class of passive dampers combining inerters with viscoelastic materials to enhance energy dissipation. Closed-form expressions for optimal design parameters are derived using statistical linearisation and H_∞ optimisation. Frequency domain analyses show that the V-shaped TIVLCD achieves peak displacement reductions of 96.93% and 96.43%, and acceleration reductions of 78.40% and 81.82%, compared to TLCD and TLCDI, respectively. Time history analyses under real earthquake ground motions reveal displacement reductions of 27.35% and 29.36%, and acceleration reductions of 22.99% and 27.17%, for U-shaped and V-shaped TIVLCDs relative to TLCDI. These improvements are attributed to the enhanced coupling between inertial, viscoelastic, and gravitational effects. The findings demonstrate that TIVLCDs, particularly the V-shaped design, provide significantly better vibration and acceleration mitigation than existing solutions, establishing them as an effective and adaptable tool for passive structural control under seismic loading.

1. Introduction

Structural vibrations present significant challenges in various engineering applications, particularly in high-rise buildings, bridges, and offshore structures subjected to dynamic excitations such as wind, seismic forces, and wave loads [1]. To mitigate these vibrations and improve structural resilience, numerous passive, semi-active, and active control mechanisms have been explored [2]. Among these, Tuned Liquid Column Dampers (TLCDs) [3] have gained popularity due to their cost-effectiveness, simplicity, and ability to dissipate energy through liquid motion [4]. However, TLCDs rely primarily on liquid sloshing [5], which limits their performance, particularly in balancing inertial and damping forces [6]. To overcome these limitations, Tuned Liquid Column Dampers with Inertia (TLCDIs) have been introduced, integrating inerters to enhance energy dissipation and extend the damping bandwidth [7]. Despite these improvements, TLCDs and TLCDIs still exhibit suboptimal performance under varying excitation conditions, necessitating further enhancements in damping strategies [8].

Recent research efforts have focused on improving passive damping mechanisms by enhancing the interaction between inertia, damping, and restoring forces to maximise vibration suppression [9]. Various modifications to TLCDs have been explored, including nonlinear TLCDs, hybrid liquid column dampers, and coupled inerter-based damping systems [10]. Additionally, H_∞ optimisation techniques and statistical linearisation methods have been used to determine optimal tuning parameters [11–13]. The integration of

* Corresponding author.
E-mail address: Sudip.Chowdhury@glasgow.ac.uk (S. Chowdhury).

https://doi.org/10.1016/j.jsv.2025.119319
Received 17 March 2025; Received in revised form 27 June 2025; Accepted 30 June 2025
Available online 10 July 2025

viscoelastic materials into vibration control devices has also been investigated, offering additional energy dissipation and frequency-dependent damping properties [14]. Furthermore, advancements in metamaterials and AI-driven optimisation have shown potential for enhancing vibration absorbers [15]. However, despite these developments, a comprehensive solution that combines inerters, viscoelasticity, and liquid column dynamics for enhanced damping remains unexplored [16].

A significant gap in the existing literature is the lack of a unified framework that systematically integrates inerters with viscoelastic liquid column dampers [17]. While TLCDs and TLCDIs have been widely studied, no prior research has effectively incorporated viscoelastic damping into liquid column-based vibration control systems [18]. Additionally, many optimisation studies rely on empirical tuning without deriving closed-form solutions for optimal parameters, which limits their generalisability [19]. Furthermore, there is limited research comparing the performance of different geometric configurations (e.g., U-shaped vs. V-shaped dampers) in liquid column damping systems, leaving a gap in understanding how design choices influence damping efficiency [20].

To address this gap, this paper introduces Tuned Inerter Viscoelastic Liquid Column Dampers (TIVLCDs), which integrate inerters, viscoelasticity, and liquid column dynamics into a single damping system. By employing statistical linearisation and H_∞ optimisation, closed-form optimal design parameters are derived to maximise vibration suppression while ensuring robustness across a range of structural applications. A comparative analysis of U-shaped and V-shaped TIVLCD configurations is conducted to evaluate their effectiveness and identify the most efficient geometric arrangement for enhanced damping performance. This comprehensive framework integrates inerter dynamics, viscoelastic damping, and liquid column motion to improve the efficiency of liquid column dampers in structural vibration control. A detailed numerical investigation is performed to assess the frequency response, displacement, and acceleration reduction capabilities of both configurations, benchmarked against conventional TLCD and TLCDI systems. Additionally, time history analyses under real earthquake ground motions are carried out to evaluate the dampers' performance in realistic seismic conditions.

2. Structural model and governing equations of motion

Tuned Inerter Viscoelastic Liquid Column Dampers (TIVLCDs) integrate inerters, viscoelastic materials, and liquid column dynamics to enhance vibration suppression. Unlike traditional TLCDs and TLCDIs, which rely primarily on liquid motion for energy dissipation, TIVLCDs leverage additional inertial amplification and frequency-dependent damping for improved efficiency. The interaction between these components ensures optimal dissipation of vibrational energy while maintaining adaptability across different structural applications. In the proposed TIVLCD configurations, the inerter is functionally integrated such that one terminal is anchored to the structure while the other is coupled to the internal motion of the damper, specifically the sloshing liquid column. This arrangement ensures that structural vibrations induce relative acceleration across the inerter terminals, enabling the generation of inertial forces that amplify the effective mass of the system and enhance energy dissipation. The governing equations of motion are derived to capture the coupled effects of these elements, providing a robust analytical framework for performance evaluation. The subsequent sections present a detailed formulation of the equations for both U-shaped and V-shaped configurations, highlighting their relative advantages in mitigating structural vibrations.

2.1. U-shaped TIVLCD

The U-shaped TIVLCD is installed at the top of an SDOF system to control its dynamic responses. The structural diagram of this controlled SDOF system is shown in Fig. 1. Newton's second law is employed to derive the governing equations of motion of the controlled SDOF system. Accordingly, the equation of motion of the coupled SDOF system is derived as

$$m_s\ddot{x}_s + c_s\dot{x}_s + k_s x_s - \int_{-\infty}^{t} \Xi\,(t-\tau)\,\dot{y}_d\,(\tau)\,\mathrm{d}\tau - k_d y_d = -m_s\ddot{x}_g \tag{1}$$

where $x_s = v_s - x_g$ and $y_d = v_d - v_s$ define the relative displacements of the SDOF system and the damper. By considering the same approach, the governing equations of motion of the damper in horizontal and vertical directions are derived as

$$\begin{aligned} &m_{eq}\ddot{x}_s + m_{eq}\ddot{y}_d + \rho AB\ddot{u}_d + k_d y_d + \textstyle\int_{-\infty}^{t} \Xi\,(t-\tau)\,\dot{y}_d\,(\tau)\,\mathrm{d}\tau = -\left(\rho AL + m_d\right)\ddot{x}_g \\ &\rho AB\ddot{x}_s + \rho AB\ddot{y}_d + \rho AL\ddot{u}_d + \frac{1}{2}\rho A\xi|\dot{u}_d|\dot{u}_d + \rho AL\underbrace{\frac{2g}{L}}_{\omega_d^2} u_d = -\rho AB\ddot{x}_g \end{aligned} \tag{2}$$

where u_d defines the relative deflection of the liquid inside the damper. $\Xi(t) = k_v e^{-\frac{k_v t}{c_v}}$ defines the hereditary function [21,22]. The hereditary function has been substituted in Eq. (1) and the first expression of Eq. (2). Accordingly, the governing equations of motion are derived as

$$\begin{aligned} &m_s\ddot{x}_s + c_s\dot{x}_s + k_s x_s - \int_0^{\infty} k_v e^{-\left(\frac{k_v}{c_v}\right)(t-\tau)}\,\dot{y}_d\,(\tau)\,\mathrm{d}\tau - k_d y_d = -m_s\ddot{x}_g \\ &m_{eq}\ddot{x}_s + m_{eq}\ddot{y}_d + \rho AB\ddot{u}_d + k_d y_d + \int_0^{\infty} k_v e^{-\left(\frac{k_v}{c_v}\right)(t-\tau)}\,\dot{y}_d\,(\tau)\,\mathrm{d}\tau = -\left(\rho AL + m_d\right)\ddot{x}_g \end{aligned} \tag{3}$$

$m_{eq} = \rho AL + m_d + m_h$ defines the total effective mass of the U-shaped TIVLCD. ρ defines the density of the liquid. A defines the cross-sectional area of the liquid column. L defines the total length of the liquid column. B defines the horizontal length of the

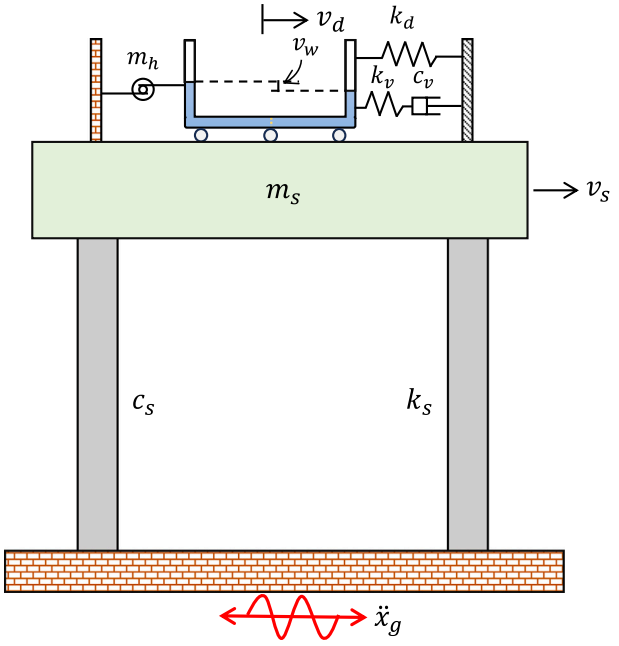

Fig. 1. A SDOF system is controlled by U-shaped TIVLCD subjected to base excitations.

damper. To solve the above equations in the frequency domain, the steady-state solutions are considered as $x_s = X_s e^{i\omega t}$, $y_d = Y_d e^{i\omega t}$, $u_d = U_d e^{i\omega t}$, and $\ddot{x}_g = X_g e^{i\omega t}$. The liquid inside the container has been formulated by the modulus function and the mathematical formulation is nonlinear. The nonlinear term in the third expression of Eq. (2) needs to be linearised to derive the optimal design parameters for the novel dampers in terms of closed-form expression. The statistical linearisation method is employed to derive the linearise term from the nonlinear element of the equation. The error estimation has been performed analytically to define the exact value of error between the nonlinear term and the equivalent linear term.

$$\kappa = \frac{1}{2}\rho A\xi|\dot{u}_d|\dot{u}_d - \underbrace{2\rho A\xi_d}_{Z_d}\dot{u}_d \tag{4}$$

where ξ_d defines the equivalent damping ratio of the liquid. The error has been estimated as follows.

$$\frac{\partial[\kappa^2]}{\partial Z_d} = \frac{\partial\left[\left(\frac{1}{2}\rho A\xi|\dot{u}_d|\dot{u}_d - Z_d\dot{u}_d\right)^2\right]}{\partial Z_d} = 0 \tag{5}$$

where $[\bullet]$ refers to the expectation operator. It is considered that $\dot{u}_d$ has been developed in the structure due to the application of Gaussian white noise at its base. Therefore, the equivalent damping ratio ξ_d has been derived as

$$\omega_d\xi_d L = \frac{\sigma_{\dot{u}_d}\xi}{\sqrt{2\pi}} \tag{6}$$

$\sigma_{\dot{u}_d}$ has been derived through the stochastic process under random white-noise excitation, i.e., $\sigma_{\dot{u}_d} = \sigma_{\dot{u}_d}\omega_d L$. Eq. (6) has been substituted in the third expression of Eq. (2). Accordingly, the equation has been modified as

$$\rho AB\ddot{x}_s + \rho AB\ddot{y}_d + \rho AL\ddot{u}_d + 2\rho AL\xi_d\omega_d\dot{u}_d + \rho AL\underbrace{\frac{2g}{L}}_{\omega_d^2}u_d = -\rho AB\ddot{x}_g \tag{7}$$

The steady-state solutions are applied to the first two expressions of Eq. (2) and the third expression of Eq. (7). The hereditary function is converted in the frequency domain and expressed as

$$\Xi(\omega) = \frac{k_v c_v}{i\omega c_v + k_v} \tag{8}$$

$k_v = \alpha m_{eq}\omega_v^2$ defines the stiffness of the viscoelastic material. α defines the stiffness ratio for the viscoelastic material to the damper, i.e., $\alpha = k_v/k_d$. $k_d = m_{eq}\omega_v^2$ defines the stiffness of the damper. $c_v = 2m_{eq}\omega_v\xi_v$ defines the damping of the damper. In addition,

all equations of motion are divided by $m_s\ \omega_s^2$. Therefore, the matrix representation of Eqs. (3) and (7) in the frequency domain is expressed as follows.

$$\begin{bmatrix} -\Omega^2+1 & -A_{22} & 0 \\ -\mu_{eq}\Omega^2 & B_{22} & -\mu_b\Omega^2 \\ -\mu_b\Omega^2 & -\mu_b\Omega^2 & -\mu_w\Omega^2+\mu_w\Omega_d^2 \end{bmatrix} \begin{Bmatrix} X_s \\ Y_d \\ U_d \end{Bmatrix} = \begin{bmatrix} -1 \\ -\mu_w-\mu_d \\ -\mu_b \end{bmatrix} \frac{X_g}{\omega_s^2} \tag{9}$$

$$A_{22} = \frac{2\,\mathrm{i}\Omega\alpha\,\Omega_v^3\mu_{eq}^2\xi_v}{2\,\mathrm{i}\mu_{eq}\xi_v\Omega_v\Omega+\alpha\,\Omega_v^2\mu_{eq}} + \Omega_v^2\mu_{eq} \quad \text{and} \quad B_{22} = -\mu_{eq}\Omega^2 + A_{22} \tag{10}$$

$\mu_{eq} = m_{eq}/m_s = \mu_w+\mu_d+\mu_h$ defines the total effective mass ratio of the U-shaped TIVLCD. $\Omega = \omega/\omega_s$ defines the excitation frequency ratio. The mass ratio, $\mu_w = \rho AL/m_s$, quantifies the proportion of the liquid mass distributed along the total length of the container relative to the structural mass. $\mu_d = m_d/m_s$ defines the mass ratio of the damper. $\mu_h = m_h/m_s$ defines the inerter mass ratio. The mass ratio, $\mu_b = \rho AB/m_s$, quantifies the proportion of the liquid mass distributed along the horizontal length of the container relative to the structural mass. The damping of the main structure is considered zero, i.e., $\xi_s = 0$, to apply the H_∞ optimisation method. Initially, $\sigma_{\dot{u}_d}$ is considered zero to derive its exact closed-form expression through the statistics linearisation process. Accordingly, ξ_d is considered zero.

$$H_s(\Omega) = \frac{X_s}{X_g}(\omega_s^2) = \frac{N_1}{\Delta} \tag{11}$$

Further, it is considered that the controlled SDOF system is subjected to harmonic base excitation. Hence, H_∞ optimisation scheme is applied on Eq. (11) to derive optimal design parameters for TIVLCD. Eq. (11) is conceptualised and the resultant of the Eq. (11) is written as :-

$$|H_s(\Omega)| = \left|\frac{I_1}{I_2}\right| \sqrt{\frac{\frac{R_1^2}{I_1^2}+\xi_v^2}{\frac{R_2^2}{I_2^2}+\xi_v^2}} \tag{12}$$

The expressions R_1, I_1, R_2, and I_2 are derived from Eqs. (11), (A.1), and (A.2). Two constraints are derived from Eq. (12) and expressed as :-

$$\left|\frac{R_1}{I_1}\right|_\Omega = \left|\frac{R_2}{I_2}\right|_\Omega \quad \text{and} \quad \left|\frac{I_1}{I_2}\right|_{\Omega_{j,k}} = \left|\frac{I_1}{I_2}\right|_{\Omega_{j,k}} \tag{13}$$

The first expression of Eq. (13) is applied and it leads to

$$O_1\Omega^4 + O_2\Omega^2 + O_3 = 0 \tag{14}$$

$$O_1 = \left(-\mu_b^2+\mu_d\mu_w+\mu_h\mu_w+\mu_w^2\right)$$

$$O_2 = \begin{pmatrix} \alpha\,\Omega_v^2\mu_b^2\mu_d+\alpha\,\Omega_v^2\mu_b^2\mu_h+\alpha\,\Omega_v^2\mu_b^2\mu_w-\alpha\,\Omega_v^2\mu_d^2\mu_w-\alpha\,\Omega_v^2\mu_d\mu_h\mu_w \\ -2\alpha\,\Omega_v^2\mu_d\mu_w^2-\alpha\,\Omega_v^2\mu_h\mu_w^2-\alpha\,\Omega_v^2\mu_w^3-\alpha\,\Omega_v^2\mu_d\mu_w-\alpha\,\Omega_v^2\mu_h\mu_w \\ -\alpha\,\Omega_v^2\mu_w^2+\Omega_v^2\mu_b^2\mu_d+\Omega_v^2\mu_b^2\mu_h+\Omega_v^2\mu_b^2\mu_w-\Omega_v^2\mu_d^2\mu_w-\Omega_v^2\mu_d\mu_h\mu_w \\ -2\Omega_v^2\mu_d\mu_w^2-\Omega_v^2\mu_h\mu_w^2-\Omega_v^2\mu_w^3-\Omega_d^2\mu_d\mu_w-\Omega_d^2\mu_h\mu_w-\Omega_d^2\mu_w^2 \\ -\Omega_v^2\mu_d\mu_w-\Omega_v^2\mu_h\mu_w-\Omega_v^2\mu_w^2 \end{pmatrix} \tag{15}$$

$$O_3 = \begin{matrix} \alpha\,\Omega_d^2\Omega_v^2\mu_d^2\mu_w+\alpha\,\Omega_d^2\Omega_v^2\mu_d\mu_h\mu_w+2\alpha\,\Omega_d^2\Omega_v^2\mu_d\mu_w^2+\alpha\,\Omega_d^2\Omega_v^2\mu_h\mu_w^2 \\ +\alpha\,\Omega_d^2\Omega_v^2\mu_w^3+\alpha\,\Omega_d^2\Omega_v^2\mu_d\mu_w+\alpha\,\Omega_d^2\Omega_v^2\mu_h\mu_w+\alpha\,\Omega_d^2\Omega_v^2\mu_w^2+\Omega_d^2\Omega_v^2\mu_d^2\mu_w \\ +\Omega_d^2\Omega_v^2\mu_d\mu_h\mu_w+2\Omega_d^2\Omega_v^2\mu_d\mu_w^2+\Omega_d^2\Omega_v^2\mu_h\mu_w^2+\Omega_d^2\Omega_v^2\mu_w^3+\Omega_d^2\Omega_v^2\mu_w^2 \\ +\Omega_d^2\Omega_v^2\mu_d\mu_w+\Omega_d^2\Omega_v^2\mu_h\mu_w \end{matrix}$$

The second expression of Eq. (13) is applied and it leads to

$$\Omega_1^2+\Omega_2^2 = 0 \quad = 0 \tag{16}$$

Eqs. (14) and (16) are compared and the closed-form expression for the optimal frequency ratio of TIVLCD is derived as :-

$$\left(\Omega_v\right)_{\text{opt}} = \sqrt{\frac{\Omega_d^2\mu_d\mu_w+\Omega_d^2\mu_h\mu_w+\Omega_d^2\mu_w^2}{\begin{matrix}\mu_d\mu_w+\mu_h\mu_w+\mu_w^2-\alpha\,\mu_b^2\mu_d-\alpha\,\mu_b^2\mu_h-\alpha\,\mu_b^2\mu_w+\alpha\,\mu_d^2\mu_w \\ +\alpha\mu_d\mu_h\mu_w+2\alpha\mu_d\mu_w^2+\alpha\mu_h\mu_w^2+\alpha\,\mu_w^3+\alpha\mu_d\mu_w+\alpha\mu_h\mu_w \\ +\alpha\,\mu_w^2-\mu_b^2\mu_d-\mu_b^2\mu_h-\mu_b^2\mu_w+\mu_d^2\mu_w+\mu_d\mu_h\mu_w+2\mu_d\mu_w^2 \\ +\mu_h\mu_w^2+\mu_w^3\end{matrix}}} \tag{17}$$

Each root $\Omega_{1,2}^2$ is derived and expressed as :-

$$\Omega_{1,2}^2 = \pm\sqrt{\frac{\Omega_d^2\Omega_v^2\mu_w\left(\mu_d+\mu_w+1\right)\left(\mu_d+\mu_h+\mu_w\right)(\alpha+1)}{\mu_b^2-\mu_d\mu_w-\mu_h\mu_w-\mu_w^2}} \tag{18}$$

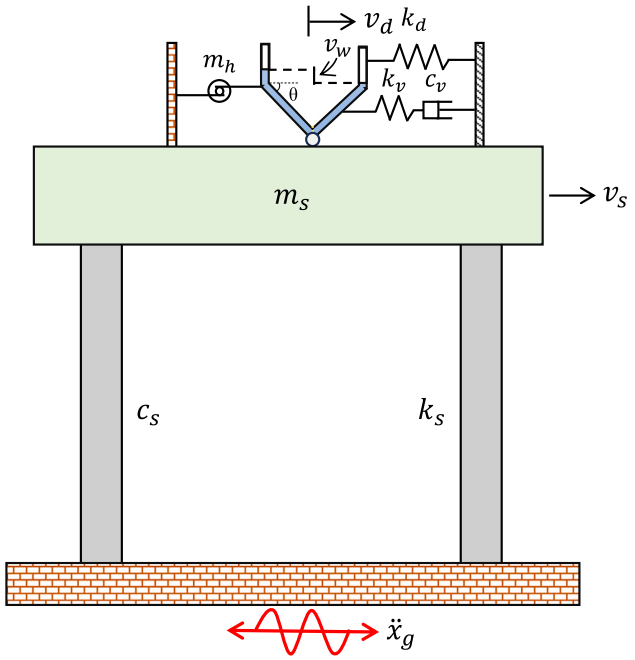

Fig. 2. A SDOF system is controlled by V-shaped TIVLCD subjected to base excitations.

The optimal damping ratio of the TIVLCD is derived using the following formulations.

$$\frac{\partial |H_s(\Omega)|^2}{\partial \Omega^2} = 0 \quad \text{and} \quad (\xi_v)_{\text{opt}} = \sqrt{\frac{\xi_{v1}^2 + \xi_{v2}^2}{2}} \tag{19}$$

The closed-form expression for $\xi_{v1,v2}$ is listed below.

$$\xi_{v1,v2} = \sqrt{\frac{Z_1}{Z_2}} \tag{20}$$

The closed-form expressions for Z_1 and Z_2 are listed in Appendix. The U-shaped Tuned Liquid Column Damper (TLCD) has several limitations that affect its efficiency in vibration suppression. Its energy dissipation relies primarily on liquid oscillation, which may be insufficient for high-frequency excitations or low-amplitude vibrations. The fixed geometry restricts frequency adaptability, making real-time tuning difficult. Additionally, an imbalance between inertial and damping effects can reduce its overall performance. Space constraints also pose a challenge, as the U-shaped configuration requires a larger footprint for installation. These drawbacks highlight the need for alternative designs, such as V-shaped TLCDs, which offer improved damping efficiency and adaptability.

2.2. V-shaped TIVLCD

The V-shaped configuration of the TIVLCD is introduced to enhance coupling between inertial and damping effects, leading to superior vibration suppression compared to the U-shaped design. By adjusting the inclination angle, the gravitational influence on the liquid motion is optimised, improving energy dissipation efficiency. This configuration allows for greater adaptability in tuning parameters, ensuring better performance under varying dynamic loads. The V-shaped TIVLCD is installed at the top of an SDOF system to control its dynamic responses. The structural diagram of this controlled SDOF system is shown in Fig. 2. Newton's second law is employed to derive the governing equations of motion of the controlled SDOF system. The following section presents the governing equations specific to the V-shaped design and its advantages over traditional damping systems. The equation of motion of the coupled SDOF system is derived as

$$m_s \ddot{x}_s + c_s \dot{x}_s + k_s x_s - \int_{-\infty}^{t} \Xi(t-\tau)\, \dot{y}_d(\tau)\, \mathrm{d}\tau - k_d y_d = -m_s \ddot{x}_g \tag{21}$$

where $x_s = v_s - x_g$ and $y_d = v_d - v_s$ define the relative displacements of SDOF system and the damper. By considering the same approach, the governing equations of motion of the damper in horizontal and vertical directions are derived as

$$\begin{aligned} m_{eq}\ddot{x}_s + m_{eq}\ddot{y}_d + m_{ev}\ddot{u}_d + k_d y_d + \int_{-\infty}^{t} \Xi(t-\tau)\,\dot{y}_d(\tau)\,\mathrm{d}\tau &= -\left(\rho AL + m_d\right)\ddot{x}_g \\ m_{ev}\ddot{x}_s + m_{ev}\ddot{y}_d + \rho AL\ddot{u}_d + \tfrac{1}{2}\rho A\xi|\dot{u}_d|\dot{u}_d + \rho AL\underbrace{\frac{(1+\sin\theta)\,g}{L}}_{\omega_d^2} u_d &= -m_{ev}\ddot{x}_g \end{aligned} \tag{22}$$

where u_d defines the relative deflection of the liquid inside the damper. $\Xi(t) = k_v e^{-\frac{k_v t}{c_v}}$ defines the hereditary function [21,22]. The hereditary function has been substituted in Eq. (21) and the first expression of Eq. (22). Accordingly, the governing equations of motion are derived as

$$\begin{aligned} m_s\ddot{x}_s + c_s\dot{x}_s + k_s x_s - \int_0^{\infty} k_v e^{-\left(\frac{k_v}{c_v}\right)(t-\tau)}\dot{y}_d(\tau)\,\mathrm{d}\tau - k_d y_d &= -m_s\ddot{x}_g \\ m_{eq}\ddot{x}_s + m_{eq}\ddot{y}_d + m_{ev}\ddot{u}_d + k_d y_d + \int_0^{\infty} k_v e^{-\left(\frac{k_v}{c_v}\right)(t-\tau)}\dot{y}_d(\tau)\,\mathrm{d}\tau &= -\left(\rho AL + m_d\right)\ddot{x}_g \end{aligned} \tag{23}$$

$m_{eq} = \rho AL + m_d + m_h$ defines the total effective mass of the V-shaped TIVLCD. $m_{ev} = \rho A\left(L - |u_d|\right)\cos\theta$ defines the total mass of the liquid inside the V-shaped container. ρ defines the density of the liquid. A defines the cross-sectional area of the liquid column. L defines the total length of the liquid column. B defines the horizontal length of the damper. The hereditary function is converted in the frequency domain and expressed as

$$\Xi(\omega) = \frac{k_v c_v}{\mathrm{i}\omega c_v + k_v} \tag{24}$$

$k_v = \alpha m_{eq}\omega_v^2$ defines the stiffness of the viscoelastic material. α defines the stiffness ratio for the viscoelastic material to the damper, i.e., $\alpha = k_v/k_d$. $k_d = m_{eq}\omega_v^2$ defines the stiffness of the damper. $c_v = 2m_{eq}\omega_v\xi_v$ defines the damping of the damper. By substituting the steady-state solutions, the matrix representation of Eq. (23) and the second expression of Eq. (22) in the frequency domain is expressed as follows.

$$\begin{bmatrix} -\Omega^2 + 1 & -A_{22} & 0 \\ -\mu_{eq}\Omega^2 & B_{22} & -\cos\theta\mu_w\Omega^2 \\ -\cos\theta\mu_w\Omega^2 & -\cos\theta\mu_w\Omega^2 & -\mu_w\Omega^2 + \mu_w\Omega_d^2 \end{bmatrix} \begin{Bmatrix} X_s \\ Y_d \\ U_d \end{Bmatrix} = \begin{bmatrix} -1 \\ -\mu_w - \mu_d \\ -\cos\theta\mu_w \end{bmatrix} \frac{X_g}{\omega_s^2} \tag{25}$$

$$A_{22} = \frac{2\,\mathrm{i}\Omega\alpha\,\Omega_v^3\mu_{eq}^2\xi_v}{2\,\mathrm{i}\mu_{eq}\xi_v\Omega_v\Omega + \alpha\,\Omega_v^2\mu_{eq}} + \Omega_v^2\mu_{eq} \quad \text{and} \quad B_{22} = -\mu_{eq}\Omega^2 + A_{22} \tag{26}$$

$\mu_{eq} = m_{eq}/m_s = \mu_w + \mu_d + \mu_h$ defines the total effective mass ratio of the V-shaped TIVLCD. $\Omega = \omega/\omega_s$ defines the excitation frequency ratio. The mass ratio, $\mu_w = \rho AL/m_s$, quantifies the proportion of the liquid mass distributed along the total length of the container relative to the structural mass. $\mu_d = m_d/m_s$ defines the mass ratio of the damper. $\mu_h = m_h/m_s$ defines the inerter mass ratio. The mass ratio, $\mu_b = \rho AB/m_s$, quantifies the proportion of the liquid mass distributed along the horizontal length of the container relative to the structural mass. θ defines the angle of the V-shaped container. The dynamic response of the SDOF system is derived as :-

$$H_s(\Omega) = \frac{X_s}{X_g}\omega_s^2 = \frac{N_2}{\Delta_v} \tag{27}$$

The closed-form expression for N_2 is listed in Appendix. Eq. (27) is conceptualised and the resultant of the Eq. (27) is written as :-

$$|H_s(\Omega)| = \left|\frac{I_1}{I_2}\right|\sqrt{\frac{\frac{R_1^2}{I_1^2} + \xi_v^2}{\frac{R_2^2}{I_2^2} + \xi_v^2}} \tag{28}$$

The expressions R_1, I_1, R_2, and I_2 are derived from Eqs. (27) and (A.6). Two constraints are derived from Eq. (28) and expressed as :-

$$\left|\frac{R_1}{I_1}\right|_{\Omega} = \left|\frac{R_2}{I_2}\right|_{\Omega} \quad \text{and} \quad \left|\frac{I_1}{I_2}\right|_{\Omega_{j,k}} = \left|\frac{I_1}{I_2}\right|_{\Omega_{j,k}} \tag{29}$$

The first expression of Eq. (29) is applied and it leads to

$$O_1\Omega^6 + O_2\Omega^4 + O_3\Omega^2 + \Omega_d^2\Omega_v^2\mu_d + \Omega_d^2\Omega_v^2\mu_h + \Omega_d^2\Omega_v^2\mu_w = 0 \tag{30}$$

$$O_1 = \left(\left(\cos^2(\theta)\right)\mu_w - \mu_d - \mu_h - \mu_w\right)$$

$$O_2 = \begin{pmatrix} -\left(\cos^2(\theta)\right)\Omega_v^2\mu_d\mu_w - \left(\cos^2(\theta)\right)\Omega_v^2\mu_h\mu_w - \left(\cos^2(\theta)\right)\Omega_v^2\mu_w^2 \\ +\Omega_v^2\mu_d^2 + 2\Omega_v^2\mu_d\mu_h + 2\Omega_v^2\mu_d\mu_w + \Omega_v^2\mu_h^2 + 2\Omega_v^2\mu_h\mu_w + \Omega_v^2\mu_w^2 \\ -\left(\cos^2(\theta)\right)\mu_w + \Omega_d^2\mu_d + \Omega_d^2\mu_h \\ +\Omega_d^2\mu_w + \Omega_v^2\mu_d + \Omega_v^2\mu_h + \Omega_v^2\mu_w + \mu_d + \mu_h + \mu_w \end{pmatrix} \tag{31}$$

$$O_3 = \begin{pmatrix} -\Omega_d^2\Omega_v^2\mu_d^2 - 2\Omega_d^2\Omega_v^2\mu_d\mu_h - 2\Omega_d^2\Omega_v^2\mu_d\mu_w - \Omega_d^2\Omega_v^2\mu_h^2 - 2\Omega_d^2\Omega_v^2\mu_h\mu_w \\ -\Omega_d^2\Omega_v^2\mu_w^2 - \Omega_d^2\Omega_v^2\mu_d - \Omega_d^2\Omega_v^2\mu_h - \Omega_d^2\Omega_v^2\mu_w - \Omega_d^2\mu_d - \Omega_d^2\mu_h - \Omega_d^2\mu_w \\ -\Omega_v^2\mu_d - \Omega_v^2\mu_h - \Omega_v^2\mu_w \end{pmatrix}$$

$$\Omega_1^2 + \Omega_2^2 + \Omega_3^2 = \frac{\begin{matrix}\left(\Omega_v^2\mu_w^2 + \mu_w\right)\left(\sin^2(\theta)\right) - \Omega_v^2\mu_w\left(\mu_d + \mu_h\right)\left(\cos^2(\theta)\right) \\ +\left(\left(2\mu_d + 2\mu_h + 1\right)\mu_w + \left(\mu_d + \mu_h + 1\right)\left(\mu_d + \mu_h\right)\right)\Omega_v^2 \\ +\Omega_d^2\mu_w + \left(\Omega_d^2 + 1\right)\left(\mu_d + \mu_h\right)\end{matrix}}{\sin^2(\theta)\mu_w + \mu_d + \mu_h} \tag{32}$$

$$\Omega_2^2\Omega_1^2 + \Omega_3^2\Omega_1^2 + \Omega_2^2\Omega_3^2 = \frac{\left(\left(1 + \left(\mu_d + \mu_h + \mu_w + 1\right)\Omega_v^2\right)\Omega_d^2 + \Omega_v^2\right)\left(\mu_d + \mu_h + \mu_w\right)}{\sin^2(\theta)\mu_w + \mu_d + \mu_h} \tag{33}$$

$$\Omega_1^2\Omega_2^2\Omega_3^2 = \frac{\Omega_d^2\Omega_v^2\left(\mu_d + \mu_h + \mu_w\right)}{\left(\sin^2(\theta)\right)\mu_w + \mu_d + \mu_h} \tag{34}$$

The second expression of Eq. (29) is applied, and it leads to

$$\Omega_1^2 + \Omega_2^2 \quad = 0 \tag{35}$$

Eqs. (30) and (35) are compared and the closed-form expression for the optimal frequency ratio of TIVLCD is derived as :-

$$E_1\Omega_v^4 + E_2\Omega_v^2 + E_3 = 0 \tag{36}$$

$$E_1 = \begin{pmatrix} -\mu_w\left(\mu_d + \mu_h\right)\left(\cos^2(\theta)\right) + \left(\sin^2(\theta)\right)\mu_w^2 \\ +\left(2\mu_d + 2\mu_h + 1\right)\mu_w + \left(\mu_d + \mu_h + 1\right)\left(\mu_d + \mu_h\right) \\ \left(\Omega_d^2\mu_d + \Omega_d^2\mu_h + \Omega_d^2\mu_w + \Omega_d^2 + 1\right) \end{pmatrix} \tag{37}$$

$$E_2 = \begin{matrix} -2\mu_w\Omega_d^2\left(\mu_d + \mu_h\right)\left(\cos^2(\theta)\right) + \left(2\Omega_d^2\mu_w^2 + \mu_w\right)\left(\sin^2(\theta)\right) \\ +\left(\mu_d + \mu_h + \mu_w + 1\right)\left(\mu_d + \mu_h + \mu_w\right)\Omega_d^4 \\ +\left(\left(4\mu_d + 4\mu_h + 2\right)\mu_w + 2\left(\mu_d + \mu_h + 1\right)\left(\mu_d + \mu_h\right)\right)\Omega_d^2 + \mu_d + \mu_h \end{matrix} \tag{38}$$

$$E_3 = \left(\sin^2(\theta)\right)\Omega_d^2\mu_w + \Omega_d^4\mu_d + \Omega_d^4\mu_h + \Omega_d^4\mu_w + \Omega_d^2\mu_d + \Omega_d^2\mu_h \tag{39}$$

The closed-form expression for the optimal frequency ratio of TIVLCD is derived as :-

$$\left(\Omega_v\right)_{\text{opt}} = \sqrt{\frac{E_2 - \sqrt{E_2^2 - 4E_1E_3}}{2E_1}} \tag{40}$$

Each root $\Omega_{1,2}^2$ is derived and expressed as :-

$$\Omega_3^2 = \frac{\begin{matrix}\left(\Omega_v^2\mu_w^2 + \mu_w\right)\left(\sin^2(\theta)\right) - \Omega_v^2\mu_w\left(\mu_d + \mu_h\right)\left(\cos^2(\theta)\right) \\ +\left(\left(2\mu_d + 2\mu_h + 1\right)\mu_w + \left(\mu_d + \mu_h + 1\right)\left(\mu_d + \mu_h\right)\right)\Omega_v^2 \\ +\Omega_d^2\mu_w + \left(\Omega_d^2 + 1\right)\left(\mu_d + \mu_h\right)\end{matrix}}{\sin^2(\theta)\mu_w + \mu_d + \mu_h} \tag{41}$$

$$\Omega_{1,2}^2 = \pm\sqrt{\frac{\left(\left(1 + \left(\mu_d + \mu_h + \mu_w + 1\right)\Omega_v^2\right)\Omega_d^2 + \Omega_v^2\right)\left(\mu_d + \mu_h + \mu_w\right)}{\left(\sin^2(\theta)\right)\mu_w + \mu_d + \mu_h}} \tag{42}$$

The optimal damping ratio of the TIVLCD is derived using the following formulations.

$$\frac{\partial|H_s(\Omega)|^2}{\partial\Omega^2} = 0 \quad \text{and} \quad \left(\xi_v\right)_{\text{opt}} = \sqrt{\frac{\xi_{v1}^2 + \xi_{v2}^2 + \xi_{v3}^2}{3}} \tag{43}$$

3. Optimal parameter selection

The parameter study in this section is essential for optimising the performance of Tuned Inerter Viscoelastic Liquid Column Dampers (TIVLCDs) by systematically investigating the influence of key design variables. By analysing the variations in the optimal frequency ratio (Ω_v) and optimal damping ratio (ξ_v) with respect to the damper mass ratio (μ_d), this study establishes a comprehensive understanding of how different configurations affect energy dissipation efficiency. The comparison between U-shaped and V-shaped TIVLCDs highlights the superior vibration suppression capacity of the V-shaped design due to enhanced coupling between inertial and viscoelastic damping mechanisms. Additionally, the impact of the stiffness ratio (α) and inclination angle

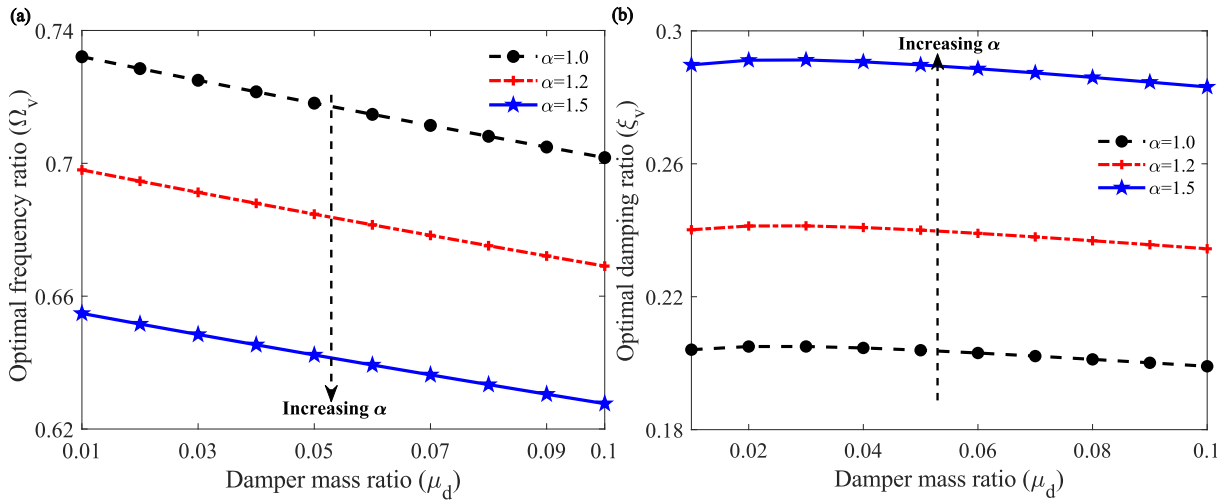

Fig. 3. Variation of optimal parameters with damper mass ratio (μ_d) for different values of α: (a) Optimal frequency ratio (Ω_v) decreases linearly with increasing μ_d, with a steeper slope observed for higher α. (b) Optimal damping ratio (ξ_v) exhibits non-linear behaviour, peaking for $\alpha = 1.5$, while remaining nearly constant for $\alpha = 1.0$. The upward and downward dashed arrows indicate the trend of "Increasing α" across the curves.

(θ) is explored to provide insights into their role in tuning the damping response for varying structural applications. The parameter selection is guided by statistical linearisation and H_∞ optimisation techniques, ensuring that the derived closed-form expressions for optimal parameters are robust and practically implementable. These findings are critical for developing advanced passive damping solutions that maximise vibration suppression in structures while maintaining design efficiency and adaptability. Fig. 3 highlights the variation of optimal parameters of U-shaped TIVLCD, specifically the optimal frequency ratio (Ω_v) and optimal damping ratio (ξ_v), with respect to the damper mass ratio (μ_d) for different values of the parameter α. In Fig. 3(a), Ω_v decreases linearly as μ_d increases, with a steeper slope observed for higher α values (1.0, 1.2, and 1.5). This trend reflects the added inertia from higher damper mass ratios, which reduces the system's effective natural frequency. The influence of α on this slope indicates that higher α values amplify the sensitivity of Ω_v to changes in μ_d, a critical consideration for applications requiring precise frequency tuning. Fig. 3(b) demonstrates a non-linear variation in ξ_v, where it remains nearly constant for $\alpha = 1.0$ but exhibits a peak for $\alpha = 1.5$ at an intermediate μ_d (0.05). This peak indicates an optimal damper mass ratio that maximises energy dissipation, while higher μ_d values may reduce efficiency due to over-damping effects. The constant behaviour of ξ_v for $\alpha = 1.0$ suggests a robust design less sensitive to μ_d variations, whereas the peak for $\alpha = 1.5$ offers enhanced damping performance, albeit requiring precise tuning. Overall, these results underscore the need to balance μ_d, α, and the desired system performance, where higher α improves peak efficiency but introduces greater design sensitivity, making these parameters critical for optimising Tuned Inerter Viscoelastic Liquid Column Dampers in various structural applications.

Fig. 4 illustrates the variation of optimal frequency ratio (Ω_v) and optimal damping ratio (ξ_v) of V-shaped TIVLCD with respect to the damper mass ratio (μ_d) for different inclination angles ($\theta = 10°, 20°, 30°$). Fig. 4(a) shows that Ω_v increases with μ_d initially, reaching a peak at an intermediate μ_d value (0.04) before gradually decreasing. Higher inclination angles (θ) lead to larger peak values of Ω_v, with $\theta = 30°$ exhibiting the highest peak. This behaviour is attributed to the coupling effects between the damper's inertia and the liquid column's motion, where increasing θ enhances the dynamic contribution of the liquid column, effectively shifting the system's optimal frequency. Fig. 4(b) reveals a sharp decline in ξ_v at low μ_d values, followed by a gradual rise and eventual stabilisation as μ_d increases. The decline is more pronounced for higher θ, reflecting a reduced damping efficiency at low damper masses due to insufficient energy dissipation. However, as μ_d increases, the stabilising effect becomes apparent, with higher θ values consistently producing slightly greater ξ_v. This trend suggests that larger inclination angles improve the damper's energy dissipation capabilities at higher mass ratios, making θ a critical design parameter for tuning both frequency and damping performance. The interplay between μ_d and θ is essential for optimising the Tuned Inerter Viscoelastic Liquid Column Dampers for applications requiring precise vibration control. The selected range of damper mass ratio ($\mu_d = 0.01$–0.1) reflects practical limits for structural applications, ensuring the damper mass remains within 1%–10% of the primary structure's mass, consistent with classical TLCD systems. The stiffness ratio ($\alpha = 1.0$–1.5) represents realistic values for viscoelastic materials used in structural damping, capturing the relative stiffness between the viscoelastic component and the main damper, as commonly adopted in TLCD, TLCDI, and Viscoelastic Tuned Mass Damper (VTMD) [21] literature.

4. Dynamic response evaluation

To evaluate the effectiveness of the proposed Tuned Inerter Viscoelastic Liquid Column Dampers (TIVLCDs), a comparative analysis of optimal design parameters is conducted. The performance of U-shaped and V-shaped TIVLCDs is assessed alongside

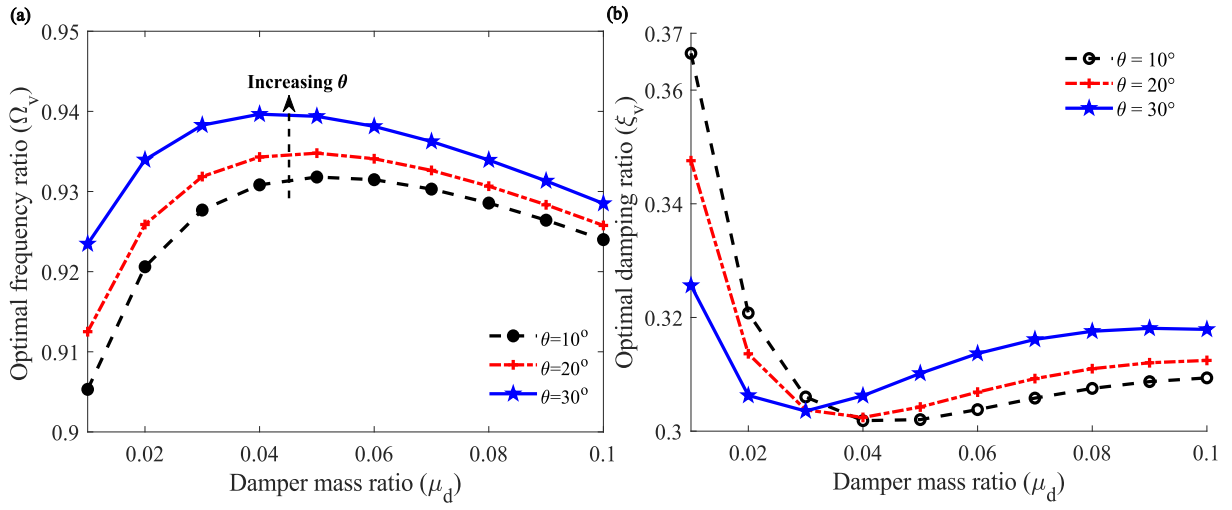

Fig. 4. Variations of (a) optimal frequency ratio (Ω_v) and (b) optimal damping ratio (ξ_v) with respect to the damper mass ratio (μ_d) for different values of θ (10°, 20°, and 30°). The graphs illustrate the dependency of Ω_v and ξ_v on the damper mass ratio, showing increasing trends with θ. Line styles (dash, dash-dot, and solid) and markers (circle, square, and star) represent different θ values for clarity.

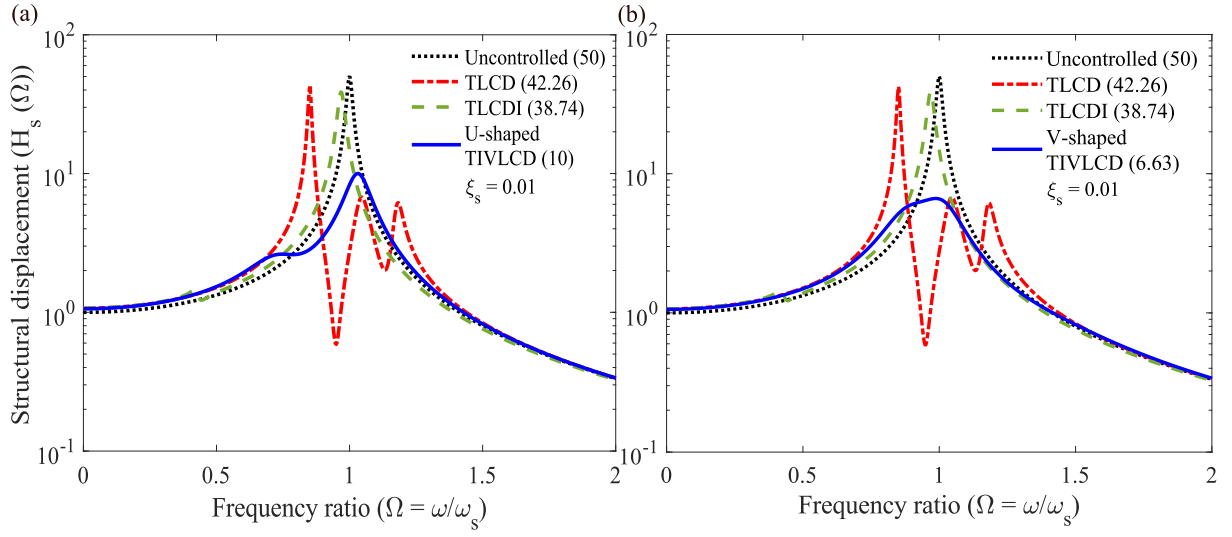

Fig. 5. Frequency response of structural displacement for systems equipped with TLCD, TLCDI, and the proposed TIVLCD under (a) U-shaped and (b) V-shaped configurations at a structural damping ratio of $\xi_s = 0.01$. The legends identify each configuration and highlight the relative performance improvements.

conventional Tuned Liquid Column Dampers (TLCDs) and Tuned Liquid Column Dampers with Inertia (TLCDIs). The optimal parameters for each damper configuration, including frequency ratio (Ω_v), damping ratio (ξ_v), liquid tuning parameter (Ω_d), and liquid damping coefficient (ξ_d), are derived through statistical linearisation and H_∞ optimisation. These parameters ensure maximum vibration suppression efficiency and structural adaptability. Table 1 presents the optimal design parameters for the proposed dampers and benchmark configurations. This comparison highlights the superior damping performance of TIVLCDs, particularly in the V-shaped configuration, which benefits from enhanced inertial and viscoelastic coupling effects. The subsequent frequency response analysis further validates the effectiveness of these optimal designs in mitigating structural vibrations.

4.1. Dynamic responses under harmonic excitation

Fig. 5 compares the frequency response of structural displacement for systems equipped with various liquid column dampers under U-shaped and V-shaped configurations at a structural damping ratio of $\xi_s = 0.01$. In Fig. 5(a), the U-shaped configuration

Table 1
Optimal parameters for the dampers.

Damper	Proposed by	Optimal design parameters			
		Ω_v	ξ_v	Ω_d	ξ_d
U-shaped TIVLCD	This study	0.71811	0.203902	1.04435	0.161587
V-shaped TIVLCD	This study	0.939382	0.310163	1.04435	0.161587
TLCDI	Matteo et al. [23]	1.8302	0.6029	0.4315	0.0150839
TLCD	Zhao et al. [24]	0.98	0	1.05	0.04

To ensure a fair comparison of dynamic response reduction capacity, the total mass ratio of each damper is kept consistent across all cases.

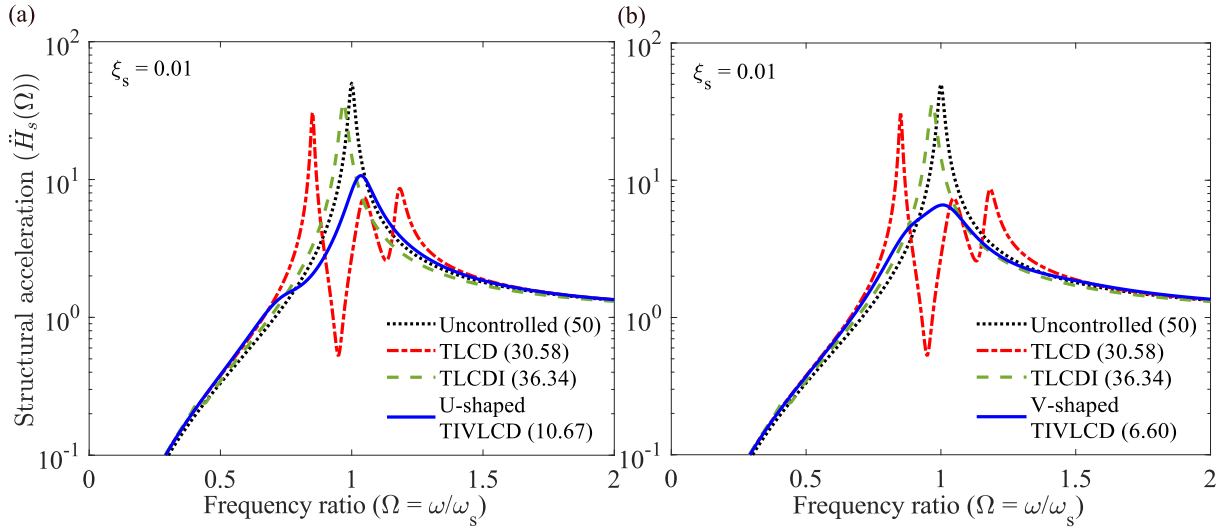

Fig. 6. The structural acceleration responses of TLCD, TLCDI, (a) U-shaped TIVLCD, and (b) V-shaped TIVLCD under harmonic excitation, illustrating the superior vibration suppression performance of the proposed TIVLCD configurations.

is analysed, where the uncontrolled response (dotted line) shows the highest peak displacement (50). The Tuned Liquid Column Damper (TLCD, red dashed line) and Tuned Liquid Column Damper with Inertia (TLCDI, green dashed line) achieve moderate displacement reductions, with maximum displacement ratios of 42.26 and 38.74, respectively. The proposed U-shaped Tuned Inerter Viscoelastic Liquid Column Damper (TIVLCD, blue solid line) significantly outperforms the conventional designs, reducing the peak displacement ratio to 10. This represents a vibration reduction capacity improvement of 76.33% compared to TLCD and 74.18% compared to TLCDI. Fig. 5(b) evaluates the V-shaped configuration under similar conditions. Here, the uncontrolled response (dotted line) again exhibits the largest peak displacement (50). The TLCD and TLCDI provide some improvement, with maximum displacement ratios of 42.26 and 38.74, respectively. However, the V-shaped TIVLCD demonstrates superior performance, reducing the peak displacement ratio to just 6.63. This corresponds to a vibration reduction capacity improvement of 84.31% compared to TLCD and 82.88% compared to TLCDI. The enhanced efficiency of the novel TIVLCD is attributed to the combined effects of inertial and viscoelastic forces, as well as the optimised liquid column motion, particularly in the V-shaped configuration. These results highlight the superior vibration reduction capacity of the TIVLCD compared to traditional dampers, validating its effectiveness for mitigating peak structural responses under dynamic excitation. Fig. 6 compares the structural acceleration responses for four damper systems: TLCD, TLCDI, U-shaped TIVLCD, and V-shaped TIVLCD. In addition, Fig. 6(a) and (b) explicitly show the acceleration responses of the U-shaped and V-shaped TIVLCDs. The maximum acceleration responses of the SDOF systems controlled by TLCD, TLCDI, U-shaped TIVLCD, and V-shaped TIVLCD are obtained as 30.58, 36.34, 10.67, and 6.60. The peak responses are compared. According to that, the acceleration response reduction capacity of U-shaped TIVLCD is 65.09% and 70.63% superior to the TLCD and TLCDI. In addition, the acceleration response reduction capacity of V-shaped TIVLCD is 78.40% and 81.82% superior to the TLCD and TLCDI. The results demonstrate that both U-shaped and V-shaped TIVLCDs exhibit significantly reduced peak responses compared to conventional TLCD and TLCDI systems. The V-shaped TIVLCD achieves the greatest reduction in resonant amplitude, attributed to the enhanced inertial coupling and geometric amplification provided by its configuration. The U-shaped TIVLCD also shows noticeable improvement over the TLCDI, highlighting the effectiveness of incorporating inertial and viscoelastic elements. These results confirm the superior vibration attenuation capability of the proposed TIVLCDs, particularly the V-shaped design, under harmonic excitation.

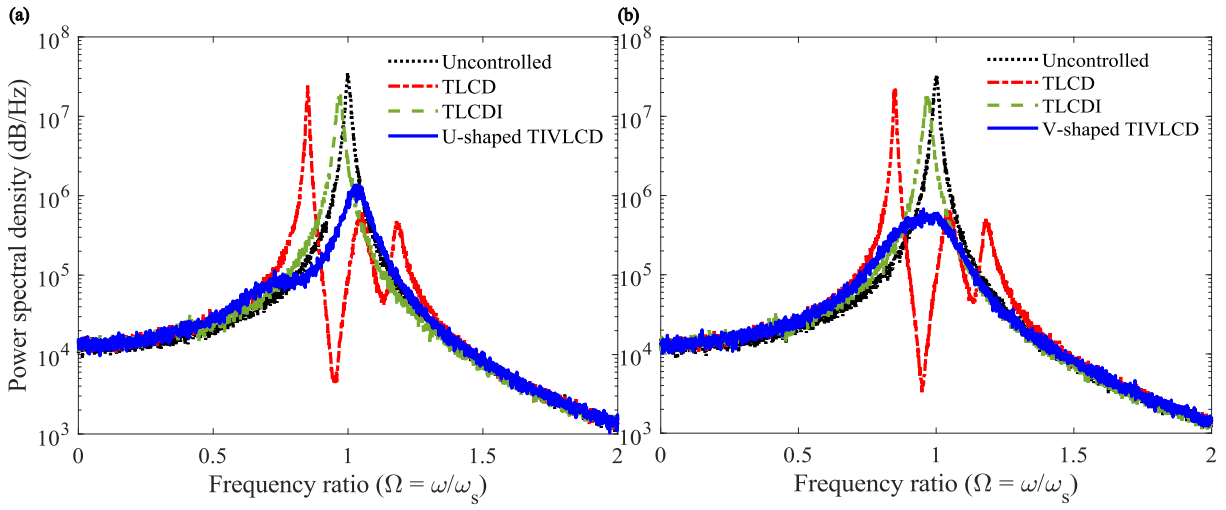

Fig. 7. Power spectral density (PSD) of structural responses for systems equipped with TLCD, TLCDI, and the proposed TIVLCD under (a) U-shaped and (b) V-shaped configurations. The legends indicate the corresponding damper types used for comparison across frequency ratios.

4.2. Randomly excited dynamic responses

Fig. 7 presents a comparison of the power spectral density (PSD) of vibration responses for various vibration control devices under harmonic excitation. Fig. 7(a) evaluates the U-shaped configurations, comparing the uncontrolled response (dotted black) with the Tuned Liquid Column Damper (TLCD, dashed red), the Tuned Liquid Column Damper with Inertia (TLCDI, dashed green), and the U-shaped Tuned Inerter Viscoelastic Liquid Column Damper (TIVLCD, solid blue). The PSD of the U-shaped TIVLCD demonstrates a significant reduction in vibration amplitudes compared to the conventional TLCD and TLCDI, particularly around the resonance frequency ($\Omega = \omega/\omega_s$), highlighting the superior vibration suppression capacity of the novel TIVLCD design. Specifically, the U-shaped configuration is analysed, where the uncontrolled response (dotted line) shows the highest peak displacement 3.4881×10^7 dB/Hz. The Tuned Liquid Column Damper (TLCD, red dashed line) and Tuned Liquid Column Damper with Inertia (TLCDI, green dashed line) achieve moderate displacement reductions, with maximum displacement ratios of 2.4364×10^7 dB/Hz and 1.9535×10^7 dB/Hz, respectively. The proposed U-shaped Tuned Inerter Viscoelastic Liquid Column Damper (TIVLCD, blue solid line) significantly outperforms the conventional designs, reducing the peak displacement ratio to 1.3615×10^6 dB/Hz. This represents a vibration reduction capacity improvement of 94.41% compared to TLCD and 93.03% compared to TLCDI. Fig. 7(b) focuses on the V-shaped configurations, showing a similar trend. The uncontrolled response exhibits the highest PSD, followed by the TLCD and TLCDI, which provide moderate vibration suppression. The V-shaped TIVLCD (solid blue line), however, achieves the most substantial reduction in PSD, demonstrating superior performance in suppressing resonance-induced vibrations. The combination of inertial and viscoelastic effects in the TIVLCD, particularly under the V-shaped configuration, enhances its ability to dissipate energy and suppress vibrations more effectively than traditional designs. The TLCD and TLCDI provide some improvement, with maximum displacement ratios of 2.2107×10^7 dB/Hz and 1.9005×10^7 dB/Hz, respectively. However, the V-shaped TIVLCD demonstrates superior performance, reducing the peak displacement ratio to just 6.7799×10^5 dB/Hz. This corresponds to a vibration reduction capacity improvement of 96.93% compared to TLCD and 96.43% compared to TLCDI. Across both configurations, the U-shaped and V-shaped TIVLCD outperform the conventional dampers, making them an effective solution for vibration control under dynamic loading conditions.

Fig. 8 examines the influence of inclination angle (θ) on the structural displacement response ($H_s(\Omega)$) and power spectral density (PSD) of the V-shaped TIVLCD system. Fig. 8(a) illustrates the structural displacement response for various inclination angles ($\theta = 10°, 20°, 30°$) as a function of the frequency ratio ($\Omega = \omega/\omega_s$). The peak displacement decreases progressively with increasing θ, from 6.9467 for $\theta = 10°$, to 6.7920 for $\theta = 20°$, and finally to 6.6362 for $\theta = 30°$. This reduction in peak displacement with larger inclination angles demonstrates the enhanced vibration mitigation capability of the system due to improved energy dissipation and optimised liquid column dynamics at higher θ. Fig. 8(b) shows the PSD of the structural response, highlighting the energy distribution across frequency ratios for the same inclination angles. The peak PSD values are noticeably reduced as θ increases, further confirming that higher inclination angles enhance the vibration suppression performance by dispersing energy more effectively. The combined effects of increased gravitational influence and improved coupling between inertial and damping forces at larger θ contribute to this enhanced performance. The peak displacement decreases progressively with increasing θ, from 7.2425×10^5 dB/Hz for $\theta = 10°$, to 6.6480×10^5 dB/Hz for $\theta = 20°$, and finally to 6.4921×10^5 dB/Hz for $\theta = 30°$. Overall, the results emphasise that increasing the inclination angle improves both displacement and spectral response, making θ a critical design parameter for optimising the system's vibration control capabilities.

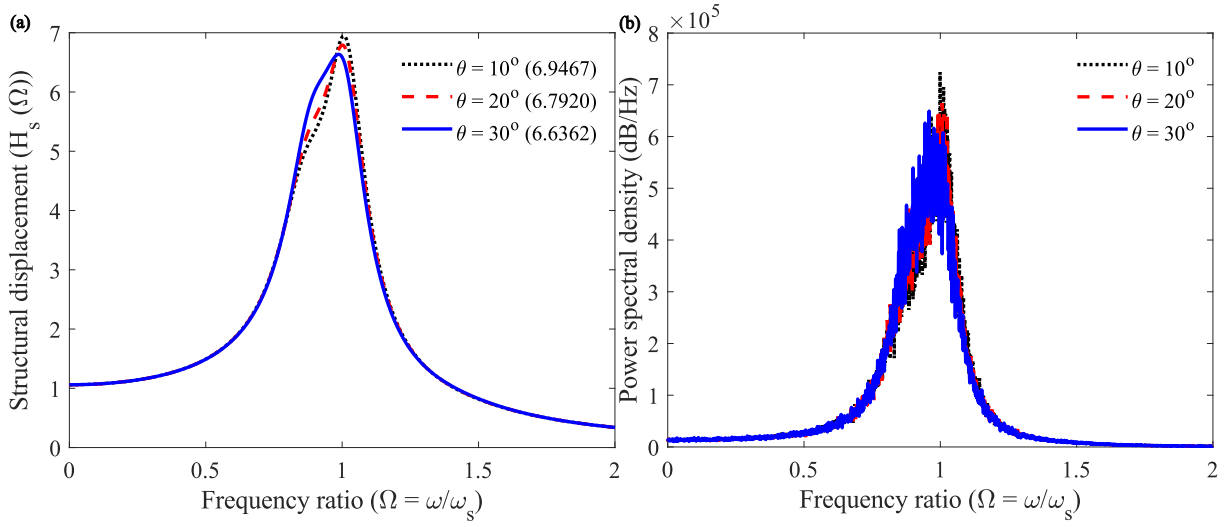

Fig. 8. Structural response analysis of the V-shaped TIVLCD system for different inclination angles ($\theta = 10°, 20°, 30°$). (a) Displacement response and (b) power spectral density (PSD) are shown as the functions of the frequency ratio (Ω).

Table 2
Information on the earthquake ground motion records.

Earthquake	Year	M_w	Recording station	Vs_{30} (m/s)	Component	E_s (km)	PGA,g
Irpinia, Italy-01	1980	6.9	Sturno	1000	MUL009	30.4	0.31
Superstition Hills-02	1987	6.5	Parachute test site	349	SUPERST	16.0	0.42
Loma Prieta	1989	6.9	LOMAP	371	HEC000	27.2	0.38
Erzican, Turkey	1992	6.7	Erzincan 11	275	ERZIKAN	9.0	0.49
Cape Mendocino	1992	7.0	CAPEMEND	713	NIS090	4.5	0.63
Landers	1992	7.3	Lucerne	685	LANDERS	44.0	0.79
Northridge-01	1994	6.7	Rinaldi receiving sta	282	NORTHR	10.9	0.87
Kocaeli, Turkey	1999	7.5	Izmit	811	KOCAELI	5.3	0.22
Chi-Chi, Taiwan	1999	7.6	TCU065	306	CHICHI	26.7	0.82
Chi-Chi, Taiwan	1999	7.6	TCU102	714	CHICHI	45.6	0.29
Duzce, Turkey	1999	7.1	Duzce	276	DUZCE	1.6	0.52

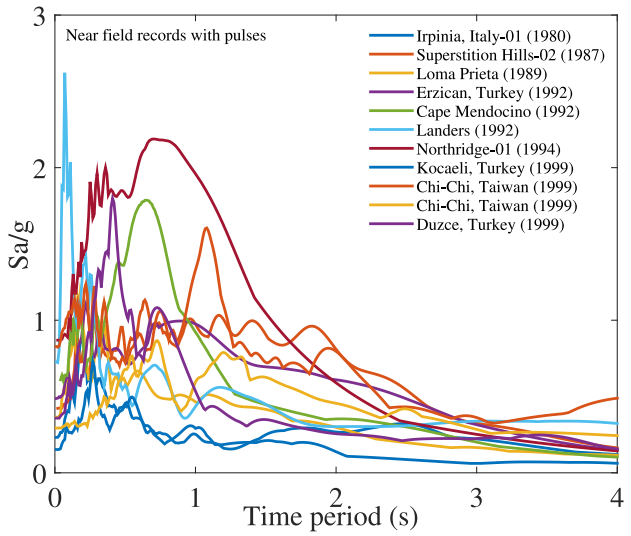

Fig. 9. The response spectra of the earthquake ground motion records are plotted considering 5% damping.

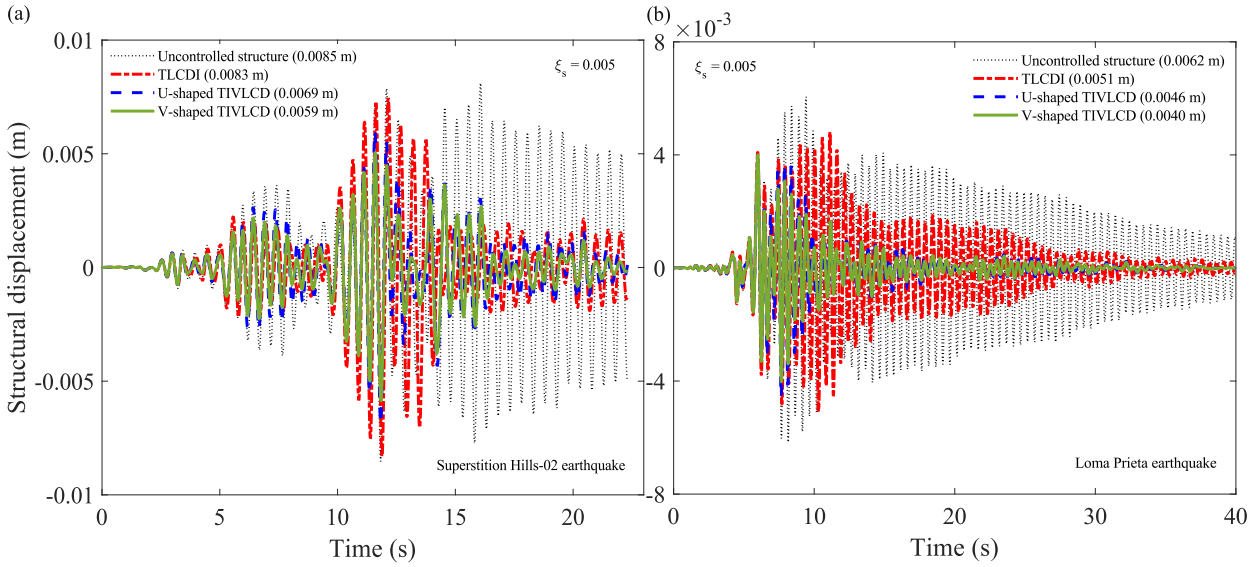

Fig. 10. The structural displacements of the SDOF systems controlled by TLCDI, U-shaped TIVLCD, and V-shaped TIVLCD under (a) Superstition Hills-02 and (b) Loma Prieta earthquakes.

4.3. Time history results

The earthquake records obtained from PEER Berkeley [25] (see Table 2) are applied as base excitations to the controlled SDOF systems for conducting the time history analysis. This analysis is carried out using the Newmark-beta method. The SDOF system is assumed to have a mass of 3000 tons and a time period of 0.5 s. The damping of the main structure is considered to be 0.005, i.e. $\xi_s = 0.005$. The selected earthquake records are used to generate the response spectra for each case. These spectra are then analysed to understand the characteristics of the earthquakes, as illustrated in the graph shown in Fig. 9. Fig. 10 presents a comparative analysis of the time–history structural displacements of an SDOF system subjected to two representative earthquake records, Fig. 10(a) Superstition Hills-02 and Fig. 10(b) Loma Prieta, under different damping configurations: uncontrolled, TLCDI, U-shaped TIVLCD, and V-shaped TIVLCD. In both subfigures, the uncontrolled structure exhibits the highest peak displacement, emphasising the system's vulnerability in the absence of supplemental damping. The addition of a TLCDI marginally reduces peak responses but fails to effectively suppress long-duration vibrations, particularly in the resonant phase of the excitation. The U-shaped TIVLCD (blue dashed line) provides a noticeable improvement by lowering both the peak and sustained oscillations due to its combined viscoelastic and inertial damping effects. The V-shaped TIVLCD (solid green line) demonstrates the most effective vibration control across both earthquake events. It consistently achieves the lowest peak displacements, 0.0059 m for Superstition Hills-02 and 0.0040 m for Loma Prieta, surpassing both TLCDI and U-shaped TIVLCD in performance. This superior efficiency is attributed to enhanced inertial-structural coupling and gravitational amplification achieved through the V-shaped geometry, which promotes more efficient energy dissipation. Overall, Fig. 10 confirms that the proposed V-shaped TIVLCD offers substantial improvements in reducing structural displacement responses under seismic excitation, validating its potential as a high-performance passive damping device for real-world structural systems. Eq. (44) quantifies the percentage reduction in maximum structural displacement achieved by the proposed U-shaped and V-shaped TIVLCD relative to the TLCDI baseline system under seismic excitation. This performance metric is essential for evaluating the effectiveness of the TIVLCD configurations in time-domain simulations using recorded earthquake data.

$$D_{x_s}(\%) = \left(\frac{\left(x_s^{max}\right)_{\text{TLCDI}} - \left(x_s^{max}\right)_{\text{U and V-shaped TIVLCD}}}{\left(x_s^{max}\right)_{\text{TLCDI}}} \right) \times 100 \tag{44}$$

The numerator captures the absolute improvement in peak displacement response due to the inclusion of viscoelastic and geometric enhancements in the TIVLCDs, while the denominator normalises this improvement with respect to the TLCDI response. The resulting percentage offers a clear, interpretable indicator of damping performance. This metric is particularly valuable for practical structural engineering applications, where relative improvement over established damping solutions (e.g., TLCDI) directly informs design decisions. As demonstrated in Table 3 of the paper, both U- and V-shaped TIVLCDs consistently yield substantial reductions in displacement, confirming the superior energy dissipation and adaptability introduced by combining inerter, viscoelastic, and liquid column dynamics within an optimised geometry. $D_{x_s}(\%)$ defines the displacement reduction capacity of the U and V-shaped TIVLCD with respect to the TLCDI. $\left(x_s^{max}\right)_{\text{TLCDI}}$ defines the maximum displacement of the SDOF system controlled by TLCDI. $\left(x_s^{max}\right)_{\text{U and V-shaped TIVLCD}}$ defines the maximum displacements of the SDOF systems controlled by the U and V-shaped TIVLCD. The maximum displacement responses from Table 3 are substituted in Eq. (44) to evaluate the overall displacement reduction

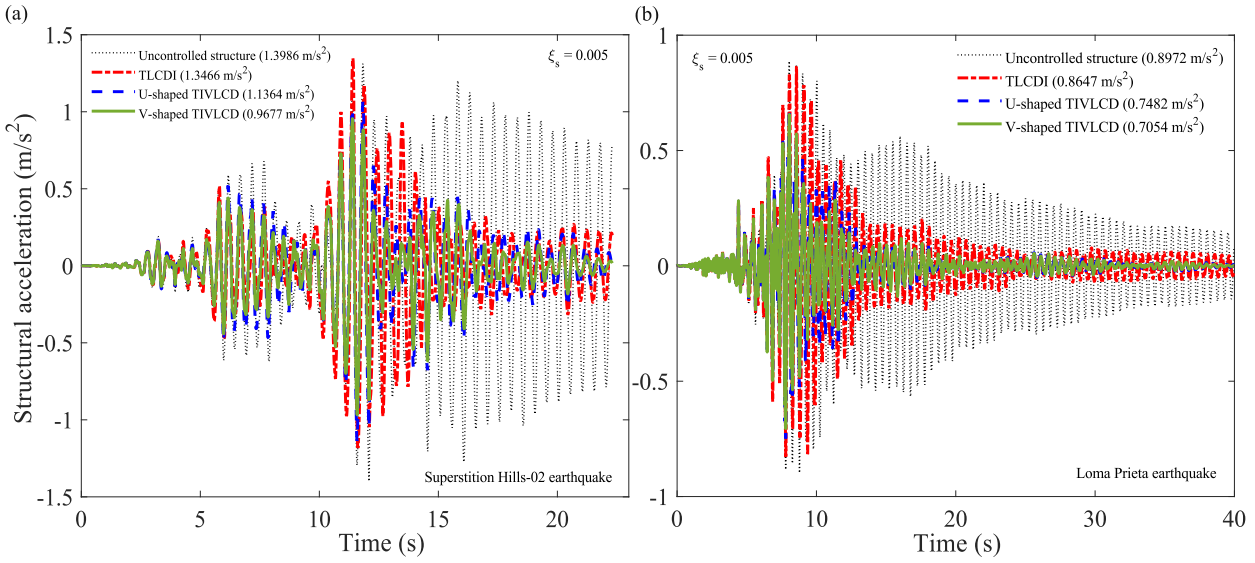

Fig. 11. The structural accelerations of the SDOF systems controlled by TLCDI, U-shaped TIVLCD, and V-shaped TIVLCD under (a) Superstition Hills-02 and (b) Loma Prieta earthquakes.

capacity of the U and V-shaped TIVLCD. Fig. 11 presents a comparative assessment of structural acceleration responses for a SDOF system subjected to two distinct earthquake excitations, (a) Superstition Hills-02 and (b) Loma Prieta, under four different control configurations: uncontrolled, TLCDI, U-shaped TIVLCD, and V-shaped TIVLCD. The damping ratio of the main structure is maintained at $\xi_s = 0.005$ in both cases to isolate the effect of the supplemental dampers. In Fig. 11(a), the uncontrolled system experiences a peak structural acceleration of 1.3986 m/s^2. The TLCDI moderately reduces this to 1.3466 m/s^2. However, the U-shaped TIVLCD achieves a more substantial reduction to 1.1364 m/s^2, while the V-shaped TIVLCD outperforms all, reducing the peak acceleration to 0.9677 m/s^2. The time history plot reveals that the V-shaped TIVLCD not only lowers the peak amplitude but also attenuates high-frequency oscillations more effectively, leading to faster energy dissipation and reduced residual vibrations. In Fig. 11(b), corresponding to the Loma Prieta earthquake, similar trends are observed. The peak acceleration for the uncontrolled system is 0.8972 m/s^2, which drops to 0.8647 m/s^2 with TLCDI control. The U-shaped and V-shaped TIVLCD configurations further reduce the accelerations to 0.7482 m/s^2 and 0.7054 m/s^2, respectively. The response curves demonstrate that both TIVLCD systems significantly reduce the structural accelerations, particularly during the peak shaking period (i.e., 10–15 s), and achieve a smoother decay phase thereafter. These results confirm that integrating viscoelastic and inerter mechanisms within liquid column dampers significantly improves acceleration suppression performance. The V-shaped configuration, benefiting from enhanced inertial coupling and geometric amplification due to its inclination angle, consistently delivers the highest reduction in structural accelerations across both earthquake events. This highlights the potential of V-shaped TIVLCDs for seismic protection in structures requiring both displacement and acceleration mitigation. Eq. (45) defines the percentage reduction in peak structural acceleration, denoted $A_{\ddot{x}_s}(\%)$, provided by the U-shaped or V-shaped Tuned Inerter Viscoelastic Liquid Column Dampers (TIVLCDs) in comparison to the TLCDI system. This performance index is essential for evaluating the effectiveness of the proposed TIVLCD configurations in mitigating inertial forces induced by seismic excitations.

$$A_{\ddot{x}_s}(\%) = \left(\frac{\left(\ddot{x}_s^{max}\right)_{\text{TLCDI}} - \left(\ddot{x}_s^{max}\right)_{\text{U and V-shaped TIVLCD}}}{\left(\ddot{x}_s^{max}\right)_{\text{TLCDI}}} \right) \times 100 \tag{45}$$

The numerator represents the absolute reduction in the maximum structural acceleration when switching from a TLCDI to a U- or V-shaped TIVLCD. The denominator normalises this reduction relative to the TLCDI's performance, yielding a percentage value that indicates how much more effective the TIVLCD is in attenuating high-frequency vibrations and peak inertial demands. This metric is crucial for assessing occupant comfort and non-structural component safety in buildings during earthquakes. As demonstrated in Table 4 of the manuscript, the V-shaped TIVLCD achieves an average acceleration reduction of 27.17%, while the U-shaped configuration achieves 22.99%, further reinforcing the improved damping performance of the V-shaped design. Eq. (45) thus offers a practical means to quantify the improvement in structural acceleration control, facilitating informed decisions in selecting damping solutions for vibration-sensitive structures. $\left(\ddot{x}_s^{max}\right)_{\text{TLCDI}}$ defines the maximum acceleration of the SDOF system controlled by TLCDI. $\left(\ddot{x}_s^{max}\right)_{\text{U and V-shaped TIVLCD}}$ defines the maximum acceleration responses of the SDOF systems controlled by the U and V-shaped TIVLCD. The maximum acceleration responses from Table 4 are substituted in Eq. (45) to evaluate the overall acceleration reduction capacity of the U and V-shaped TIVLCD.

The overall performance comparison shows that the proposed U-shaped and V-shaped TIVLCDs significantly outperform the TLCDI under various seismic excitations. Time history analyses reveal notable reductions in both structural displacement and

Table 3
The maximum displacement responses of the uncontrolled and controlled SDOF systems. The SDOF systems are controlled by TLCDI, U-shaped TIVLCD, and V-shaped TIVLCD.

Earthquake	x_s^{max} (m)				D_{x_s} (%)	
	Uncontrolled	TLCDI	U-shaped TIVLCD	V-shaped TIVLCD	U-shaped TIVLCD	V-shaped TIVLCD
Irpinia, Italy-01	0.0059	0.0059	0.0031	0.0029	47.45762712	50.84745763
Superstition Hills-02	0.0085	0.0083	0.0069	0.0059	16.86746988	28.91566265
Loma Prieta	0.0062	0.0051	0.0046	0.004	9.803921569	21.56862745
Erzican, Turkey	0.0068	0.0068	0.0057	0.0061	16.17647059	10.29411765
Cape Mendocino	0.0157	0.0116	0.0073	0.0084	37.06896552	27.5862069
Landers	0.0058	0.0045	0.004	0.0039	11.11111111	13.33333333
Northridge-01	0.0077	0.0077	0.0058	0.0055	24.67532468	28.57142857
Kocaeli, Turkey	0.0055	0.0032	0.0025	0.0025	21.875	21.875
Chi-Chi, Taiwan	0.0128	0.0098	0.0055	0.005	43.87755102	48.97959184
Chi-Chi, Taiwan	0.0074	0.005	0.0047	0.0048	6	4
Duzce, Turkey	0.0133	0.0118	0.0078	0.0073	33.89830508	38.13559322
Average	0.008690909	0.007245455	0.005263636	0.005118182	27.35257215	29.36010038

Table 4
The maximum acceleration responses of the uncontrolled and controlled SDOF systems. The SDOF systems are controlled by TLCDI, U-shaped TIVLCD, and V-shaped TIVLCD.

Earthquake	$\ddot{x}_s^{max}$ (m/s^2)				$A_{\ddot{x}_s}$ (%)	
	Uncontrolled	TLCDI	U-shaped TIVLCD	V-shaped TIVLCD	U-shaped TIVLCD	V-shaped TIVLCD
Irpinia, Italy-01	1.2212	1.06	1.0556	0.9697	0.41509434	8.518867925
Superstition Hills-02	1.3986	1.3466	1.1364	0.9677	15.60968365	28.13753156
Loma Prieta	0.8972	0.8647	0.7482	0.7054	13.47288077	18.4225743
Erzican, Turkey	0.8759	0.6323	0.5188	0.4743	17.95034003	24.98813854
Cape Mendocino	1.9038	1.8393	1.3122	1.4013	28.65764149	23.81340727
Landers	1.4073	1.1303	0.9588	0.937	15.17296293	17.10165443
Northridge-01	1.5195	1.4003	1.1237	1.0508	19.75291009	24.95893737
Kocaeli, Turkey	0.8926	0.5421	0.4147	0.3973	23.50119904	26.71093894
Chi-Chi, Taiwan	2.0188	1.4332	0.8364	0.7364	41.64108289	48.61847614
Chi-Chi, Taiwan	0.5071	0.5071	0.3329	0.3577	34.35219878	29.46164465
Duzce, Turkey	2.17	1.837	1.0587	0.9509	42.36799129	48.23625476
Average	1.346545455	1.144809091	0.863309091	0.8135	22.9903623	27.17894781

acceleration when using the new dampers. On average, the U-shaped and V-shaped TIVLCDs achieve 27.35% and 29.36% reductions in maximum displacement, and 22.99% and 27.17% reductions in peak acceleration, respectively. These improvements highlight the enhanced damping capacity introduced by the combined inerter-viscoelastic-liquid mechanism. Among the two, the V-shaped TIVLCD consistently delivers the highest performance due to its geometry, which facilitates stronger gravitational effects and inertial amplification. These results confirm the effectiveness of the proposed TIVLCDs, particularly the V-shaped configuration, as advanced passive control devices for mitigating seismic-induced structural vibrations.

5. Conclusion

This paper has presented a comprehensive investigation of Tuned Inerter Viscoelastic Liquid Column Dampers (TIVLCDs) as an advanced passive vibration control solution. Through rigorous mathematical modelling and optimisation using statistical linearisation and H_∞ techniques, closed-form expressions for optimal design parameters were derived for both U-shaped and V-shaped configurations. The frequency domain analysis demonstrates exceptional vibration suppression capabilities, with U-shaped TIVLCDs achieving peak displacement reductions of 94.41% and 93.03% compared to conventional TLCD and TLCDI systems, while V-shaped configurations exhibited even more remarkable performance with reductions of 96.93% and 96.43%, respectively. In addition, the acceleration response reduction capacity of U-shaped TIVLCD is 65.09% and 70.63% superior to the TLCD and TLCDI. The acceleration response reduction capacity of V-shaped TIVLCD is 78.40% and 81.82% superior to the TLCD and TLCDI. The time history analysis further confirms the superior performance of the proposed TIVLCD systems under seismic excitations. Compared to TLCDI, both U-shaped and V-shaped TIVLCDs consistently achieved significant reductions in maximum structural displacement across eleven real earthquake records. Notably, the V-shaped configuration demonstrated the highest displacement reduction, averaging approximately 29.36%, owing to enhanced inertial-structural coupling and geometric amplification effects. The acceleration response analysis further validated the effectiveness of the TIVLCDs, with the V-shaped design achieving the lowest peak accelerations and faster decay of vibrations. These findings underscore the practical potential of the proposed dampers in improving the seismic resilience of structures through efficient passive energy dissipation.

The novelty of this research lies in several key advances: First, the integration of inerters with viscoelastic materials creates a synergistic damping mechanism that significantly expands the effective frequency bandwidth compared to traditional liquid column dampers. Second, the derivation of exact closed-form expressions for optimal parameters enables straightforward practical implementation while ensuring robust performance. Third, the innovative V-shaped configuration maximises the coupling between inertial and damping forces, resulting in unprecedented vibration suppression efficiency. Fourth, the comprehensive frequency response analysis provides deep insights into the dynamic behaviour across different geometric configurations and operating conditions. Fifth, the statistical linearisation approach addresses nonlinear liquid motion effects while maintaining analytical tractability.

These findings have significant implications for structural vibration control across multiple engineering domains, from high-rise buildings to offshore structures. The superior performance and adaptability of TIVLCDs make them particularly valuable for applications requiring robust vibration suppression under varying dynamic loads. While this paper establishes a comprehensive theoretical and computational framework for the optimal design of TIVLCDs, experimental validation remains an important next step. Future research will involve constructing physical prototypes of both U-shaped and V-shaped TIVLCD configurations and testing them under controlled laboratory conditions using harmonic and stochastic base excitations. These experiments will assess the practical effectiveness of the closed-form optimal parameters derived through H_∞ optimisation. In addition, dynamic response simulations using real earthquake ground motions have been conducted to assess the effectiveness of the proposed dampers. These time history results also facilitate a direct basis for comparison with future experimental results subjected to the same input time histories. Future work will also extend the proposed framework to multi-degree-of-freedom systems to account for higher-mode effects and modal interactions. Future work will consider the influence of environmental factors such as temperature, which can affect fluid density and viscoelastic properties, to ensure robust performance of TIVLCDs under varying operational conditions.

CRediT authorship contribution statement

Sudip Chowdhury: Writing – review & editing, Writing – original draft, Visualization, Validation, Supervision, Software, Resources, Project administration, Methodology, Investigation, Funding acquisition, Formal analysis, Data curation, Conceptualization. **Rama Debbarma:** Writing – review & editing, Visualization, Supervision, Project administration, Methodology, Conceptualization. **Sondipon Adhikari:** Writing – review & editing, Visualization, Supervision, Resources, Project administration, Methodology, Investigation, Conceptualization.

Declaration of competing interest

The authors declare that they have no known competing financial interests or personal relationships that could have appeared to influence the work reported in this paper.

Acknowledgements

The authors would like to acknowledge the MHRD grant received from NIT Agartala during the period of this research. The authors would like to acknowledge the Post Doctoral grant received from The University of Glasgow, United Kingdom during the period of this research.

Appendix. Exact closed-form expressions from Eqs. (11), (20), and (27)

$$
\begin{aligned}
N_1 = &\begin{pmatrix}
\alpha\,\Omega^2\Omega_v^3\mu_b^2\mu_d + \alpha\,\Omega^2\Omega_v^3\mu_b^2\mu_h + \alpha\,\Omega^2\Omega_v^3\mu_b^2\mu_w - \alpha\,\Omega^2\Omega_v^3\mu_d^2\mu_w - \alpha\,\Omega^2\Omega_v^3\mu_d\mu_h\mu_w \\
-2\alpha\,\Omega^2\Omega_v^3\mu_d\mu_w^2 - \alpha\,\Omega^2\Omega_v^3\mu_h\mu_w^2 - \alpha\,\Omega^2\Omega_v^3\mu_w^3 + \alpha\,\Omega_d^2\Omega_v^3\mu_d^2\mu_w + \alpha\,\Omega_d^2\Omega_v^3\mu_d\mu_h\mu_w \\
+2\alpha\,\Omega_d^2\Omega_v^3\mu_d\mu_w^2 + \alpha\,\Omega_d^2\Omega_v^3\mu_h\mu_w^2 + \alpha\,\Omega_d^2\Omega_v^3\mu_w^3 - \alpha\,\Omega^4\Omega_v\mu_b^2 + \alpha\,\Omega^4\Omega_v\mu_d\mu_w \\
+\alpha\,\Omega^4\Omega_v\mu_h\mu_w + \alpha\,\Omega^4\Omega_v\mu_w^2 - \alpha\,\Omega^2\Omega_d^2\Omega_v\mu_d\mu_w - \alpha\,\Omega^2\Omega_d^2\Omega_v\mu_h\mu_w - \alpha\,\Omega^2\Omega_d^2\Omega_v\mu_w^2 \\
-\alpha\,\Omega^2\Omega_v^3\mu_d\mu_w - \alpha\,\Omega^2\Omega_v^3\mu_h\mu_w - \alpha\,\Omega^2\Omega_v^3\mu_w^2 + \alpha\,\Omega_d^2\Omega_v^3\mu_d\mu_w + \alpha\,\Omega_d^2\Omega_v^3\mu_h\mu_w \\
+\alpha\,\Omega_d^2\Omega_v^3\mu_w^2
\end{pmatrix} \\
&+ \mathrm{i}\xi_v\begin{pmatrix}
2\alpha\,\Omega^3\Omega_v^2\mu_b^2\mu_d + 2\alpha\,\Omega^3\Omega_v^2\mu_b^2\mu_h + 2\alpha\,\Omega^3\Omega_v^2\mu_b^2\mu_w - 2\alpha\,\Omega^3\Omega_v^2\mu_d^2\mu_w + 2\Omega\,\Omega_d^2\Omega_v^2\mu_d^2\mu_w \\
+2\Omega^5\mu_d\mu_w - 2\alpha\,\Omega^3\Omega_v^2\mu_d\mu_h\mu_w - 4\alpha\,\Omega^3\Omega_v^2\mu_d\mu_w^2 - 2\alpha\,\Omega^3\Omega_v^2\mu_h\mu_w^2 - 2\alpha\,\Omega^3\Omega_v^2\mu_w^3 \\
+2\alpha\Omega\,\Omega_d^2\Omega_v^2\mu_d^2\mu_w + 2\alpha\Omega\,\Omega_d^2\Omega_v^2\mu_d\mu_h\mu_w + 4\alpha\Omega\,\Omega_d^2\Omega_v^2\mu_d\mu_w^2 + 2\alpha\Omega\,\Omega_d^2\Omega_v^2\mu_h\mu_w^2 \\
+2\alpha\Omega\,\Omega_d^2\Omega_v^2\mu_w^3 - 2\alpha\,\Omega^3\Omega_v^2\mu_d\mu_w - 2\alpha\,\Omega^3\Omega_v^2\mu_h\mu_w - 2\alpha\,\Omega^3\Omega_v^2\mu_w^2 - 2\Omega^3\Omega_v^2\mu_h\mu_w^2 \\
+2\alpha\Omega\,\Omega_d^2\Omega_v^2\mu_d\mu_w + 2\alpha\Omega\,\Omega_d^2\Omega_v^2\mu_h\mu_w + 2\alpha\Omega\,\Omega_d^2\Omega_v^2\mu_w^2 + 2\Omega^3\Omega_v^2\mu_b^2\mu_d - 2\Omega^3\Omega_v^2\mu_w^3 \\
+2\Omega^3\Omega_v^2\mu_b^2\mu_h + 2\Omega^3\Omega_v^2\mu_b^2\mu_w - 2\Omega^3\Omega_v^2\mu_d^2\mu_w - 2\Omega^3\Omega_v^2\mu_d\mu_h\mu_w - 4\Omega^3\Omega_v^2\mu_d\mu_w^2 \\
+2\Omega\,\Omega_d^2\Omega_v^2\mu_d\mu_h\mu_w + 4\Omega\,\Omega_d^2\Omega_v^2\mu_d\mu_w^2 + 2\Omega\,\Omega_d^2\Omega_v^2\mu_h\mu_w^2 + 2\Omega\,\Omega_d^2\Omega_v^2\mu_w^3 + 2\Omega^5\mu_h\mu_w \\
+2\Omega^5\mu_w^2 - 2\Omega^3\Omega_d^2\mu_d\mu_w - 2\Omega^5\mu_b^2 - 2\Omega^3\Omega_d^2\mu_h\mu_w - 2\Omega^3\Omega_d^2\mu_w^2 - 2\Omega^3\Omega_v^2\mu_d\mu_w \\
-2\Omega^3\Omega_v^2\mu_h\mu_w - 2\Omega^3\Omega_v^2\mu_w^2 + 2\Omega\,\Omega_d^2\Omega_v^2\mu_d\mu_w + 2\Omega\,\Omega_d^2\Omega_v^2\mu_h\mu_w + 2\Omega\,\Omega_d^2\Omega_v^2\mu_w^2
\end{pmatrix}
\end{aligned}
\tag{A.1}
$$

$$
\begin{array}{c}
\alpha\,\Omega^4\Omega_v^3\mu_b^2\mu_d+\alpha\,\Omega^4\Omega_v^3\mu_b^2\mu_h+\alpha\,\Omega^4\Omega_v^3\mu_b^2\mu_w-\alpha\,\Omega^4\Omega_v^3\mu_d^2\mu_w-2\alpha\,\Omega^4\Omega_v^3\mu_d\mu_h\mu_w\\
-2\alpha\,\Omega^4\Omega_v^3\mu_d\mu_w^2-\alpha\,\Omega^4\Omega_v^3\mu_h^2\mu_w-2\alpha\,\Omega^4\Omega_v^3\mu_h\mu_w^2-\alpha\,\Omega^4\Omega_v^3\mu_w^3+\alpha\,\Omega^2\Omega_d^2\Omega_v^3\mu_d^2\mu_w\\
+2\alpha\,\Omega^2\Omega_d^2\Omega_v^3\mu_d\mu_h\mu_w+2\alpha\,\Omega^2\Omega_d^2\Omega_v^3\mu_d\mu_w^2+\alpha\,\Omega^2\Omega_d^2\Omega_v^3\mu_h^2\mu_w+2\alpha\,\Omega^2\Omega_d^2\Omega_v^3\mu_h\mu_w^2\\
+\alpha\,\Omega^2\Omega_d^2\Omega_v^3\mu_w^3-\alpha\,\Omega^6\Omega_v\mu_b^2+\alpha\,\Omega^6\Omega_v\mu_d\mu_w+\alpha\,\Omega^6\Omega_v\mu_h\mu_w+\alpha\,\Omega^6\Omega_v\mu_w^2\\
-\alpha\,\Omega^4\Omega_d^2\Omega_v\mu_d\mu_w-\alpha\,\Omega^4\Omega_d^2\Omega_v\mu_h\mu_w-\alpha\,\Omega^4\Omega_d^2\Omega_v\mu_w^2-\alpha\,\Omega^4\Omega_v^3\mu_d\mu_w-\alpha\,\Omega^4\Omega_v^3\mu_h\mu_w\\
-\alpha\,\Omega^4\Omega_v^3\mu_w^2+\alpha\,\Omega^2\Omega_d^2\Omega_v^3\mu_d\mu_w+\alpha\,\Omega^2\Omega_d^2\Omega_v^3\mu_h\mu_w+\alpha\,\Omega^2\Omega_d^2\Omega_v^3\mu_w^2+\alpha\,\Omega^4\Omega_v\mu_b^2\\
-\alpha\,\Omega^4\Omega_v\mu_d\mu_w-\alpha\,\Omega^4\Omega_v\mu_h\mu_w-\alpha\,\Omega^4\Omega_v\mu_w^2+\alpha\,\Omega^2\Omega_d^2\Omega_v\mu_d\mu_w+\alpha\,\Omega^2\Omega_d^2\Omega_v\mu_h\mu_w\\
+\alpha\,\Omega^2\Omega_d^2\Omega_v\mu_w^2+\alpha\,\Omega^2\Omega_v^3\mu_d\mu_w+\alpha\,\Omega^2\Omega_v^3\mu_h\mu_w+\alpha\,\Omega^2\Omega_v^3\mu_w^2-\alpha\,\Omega_d^2\Omega_v^3\mu_d\mu_w\\
-\alpha\,\Omega_d^2\Omega_v^3\mu_h\mu_w-\alpha\,\Omega_d^2\Omega_v^3\mu_w^2
\end{array}
$$

$$
\Delta=\begin{pmatrix}
2\alpha\,\Omega^5\Omega_v^2\mu_b^2\mu_d+2\alpha\,\Omega^5\Omega_v^2\mu_b^2\mu_h+2\alpha\,\Omega^5\Omega_v^2\mu_b^2\mu_w-2\alpha\,\Omega^5\Omega_v^2\mu_d^2\mu_w-2\alpha\,\Omega^5\Omega_v^2\mu_v^3\\
-4\alpha\,\Omega^5\Omega_v^2\mu_d\mu_h\mu_w-4\alpha\,\Omega^5\Omega_v^2\mu_d\mu_w^2-2\alpha\,\Omega^5\Omega_v^2\mu_h^2\mu_w-4\alpha\,\Omega^5\Omega_v^2\mu_h\mu_w^2\\
+2\alpha\,\Omega^3\Omega_d^2\Omega_v^2\mu_d^2\mu_w+4\alpha\,\Omega^3\Omega_d^2\Omega_v^2\mu_d\mu_h\mu_w+4\alpha\,\Omega^3\Omega_d^2\Omega_v^2\mu_d\mu_w^2+2\alpha\,\Omega^3\Omega_d^2\Omega_v^2\mu_h^2\mu_w\\
+4\alpha\,\Omega^3\Omega_d^2\Omega_v^2\mu_h\mu_w^2+2\alpha\,\Omega^3\Omega_d^2\Omega_v^2\mu_w^3-2\alpha\,\Omega^5\Omega_v^2\mu_d\mu_w-2\alpha\,\Omega^5\Omega_v^2\mu_h\mu_w\\
-2\alpha\,\Omega^5\Omega_v^2\mu_w^2+2\alpha\,\Omega^3\Omega_d^2\Omega_v^2\mu_d\mu_w+2\alpha\,\Omega^3\Omega_d^2\Omega_v^2\mu_h\mu_w+2\alpha\,\Omega^3\Omega_d^2\Omega_v^2\mu_w^2\\
+2\Omega^5\Omega_v^2\mu_b^2\mu_d+2\Omega^5\Omega_v^2\mu_b^2\mu_h+2\Omega^5\Omega_v^2\mu_b^2\mu_w-2\Omega^5\Omega_v^2\mu_d^2\mu_w-4\Omega^5\Omega_v^2\mu_d\mu_h\mu_w\\
-4\Omega^5\Omega_v^2\mu_d\mu_w^2-2\Omega^5\Omega_v^2\mu_h^2\mu_w-4\Omega^5\Omega_v^2\mu_h\mu_w^2-2\Omega^5\Omega_v^2\mu_w^3+2\Omega^3\Omega_d^2\Omega_v^2\mu_d^2\mu_w\\
+4\Omega^3\Omega_d^2\Omega_v^2\mu_d\mu_h\mu_w+4\Omega^3\Omega_d^2\Omega_v^2\mu_d\mu_w^2+2\Omega^3\Omega_d^2\Omega_v^2\mu_h^2\mu_w+4\Omega^3\Omega_d^2\Omega_v^2\mu_h\mu_w^2\\
-2\Omega^7\mu_b^2+2\Omega^7\mu_d\mu_w+2\Omega^7\mu_h\mu_w+2\Omega^7\mu_w^2-2\Omega^5\Omega_d^2\mu_d\mu_w-2\Omega^5\Omega_d^2\mu_h\mu_w\\
-2\Omega^5\Omega_d^2\mu_w^2-2\Omega^5\Omega_v^2\mu_d\mu_w-2\Omega^5\Omega_v^2\mu_h\mu_w-2\Omega^5\Omega_v^2\mu_w^2+2\Omega^3\Omega_d^2\Omega_v^2\mu_d\mu_w\\
+2\Omega^3\Omega_d^2\Omega_v^2\mu_w^2+2\alpha\,\Omega^3\Omega_v^2\mu_d\mu_w+2\alpha\,\Omega^3\Omega_v^2\mu_h\mu_w+2\alpha\,\Omega^3\Omega_v^2\mu_w^2+2\Omega^3\Omega_d^2\Omega_v^2\mu_w^3\\
-2\alpha\Omega\,\Omega_d^2\Omega_v^2\mu_h\mu_w-2\alpha\Omega\,\Omega_d^2\Omega_v^2\mu_w^2+2\Omega^5\mu_b^2-2\Omega^5\mu_d\mu_w-2\Omega^5\mu_h\mu_w\\
-2\Omega^5\mu_w^2+2\Omega^3\Omega_d^2\mu_d\mu_w+2\Omega^3\Omega_d^2\mu_h\mu_w+2\Omega^3\Omega_d^2\mu_w^2+2\Omega^3\Omega_v^2\mu_d\mu_w\\
+2\Omega^3\Omega_v^2\mu_w^2-2\Omega\,\Omega_d^2\Omega_v^2\mu_d\mu_w-2\Omega\,\Omega_d^2\Omega_v^2\mu_h\mu_w-2\Omega\,\Omega_d^2\Omega_v^2\mu_w^2+2\Omega^3\Omega_d^2\Omega_v^2\mu_h\mu_w\\
-2\alpha\Omega\,\Omega_d^2\Omega_v^2\mu_d\mu_w+2\Omega^3\Omega_v^2\mu_h\mu_w
\end{pmatrix}
$$

(A.2)

$$
Z_1=\alpha^2\begin{pmatrix}
\left(\mu_w^2+\left(\mu_d+\mu_h\right)\mu_w-\mu_b^2\right)\Omega_{1,2}^6\\
-\begin{pmatrix}
\mu_w^3\Omega_v^2+\left(\left(2\mu_d+2\mu_h+1\right)\Omega_v^2+\Omega_d^2+1\right)\mu_w^2\\
+\left(\begin{pmatrix}\mu_d^2+\left(2\mu_h+1\right)\mu_d\\-\mu_b^2+\mu_h^2+\mu_h\end{pmatrix}\Omega_v^2\right)\mu_w\\
+\left(\Omega_d^2+1\right)\left(\mu_d+\mu_h\right)\\
-\left(1+\left(\mu_d+\mu_h\right)\Omega_v^2\right)\mu_b^2
\end{pmatrix}\Omega_{1,2}^4\\
+\mu_w\begin{pmatrix}\mu_w\Omega_d^2\Omega_v^2+\Omega_d^2\\+\left(1+\left(\mu_d+\mu_h+1\right)\Omega_d^2\right)\Omega_v^2\end{pmatrix}\left(\mu_d+\mu_h+\mu_w\right)\Omega_{1,2}^2\\
-\mu_w\Omega_d^2\Omega_v^2\left(\mu_d+\mu_h+\mu_w\right)
\end{pmatrix}^2\Omega_v^2
$$

(A.3)

$$
Z_2=4\begin{pmatrix}
\left(-\mu_w^2+\left(-\mu_d-\mu_h\right)\mu_w+\mu_b^2\right)\Omega_{1,2}^6\\
+\begin{pmatrix}
(\alpha+1)\,\Omega_v^2\mu_w^3\\
+\left(\begin{pmatrix}2\left(\mu_d+\mu_h+\frac{1}{2}\right)(\alpha+1)\,\Omega_v^2\\+\Omega_d^2+1\end{pmatrix}\mu_w^2\right)\\
+\left(\begin{pmatrix}-\mu_d^2+\left(-2\mu_h-1\right)\mu_d\\+\mu_b^2-\mu_h^2-\mu_h\end{pmatrix}\mu_w\right)\\
(\alpha+1)\,\Omega_v^2\\
+\left(\Omega_d^2+1\right)\left(\mu_d+\mu_h\right)\\
-\left(1+\left(\mu_d+\mu_h\right)(\alpha+1)\,\Omega_v^2\right)\mu_b^2
\end{pmatrix}\Omega_{1,2}^4\\
-\begin{pmatrix}\Omega_d^2\Omega_v^2(\alpha+1)\,\mu_w\\+\left(1+\left(\mu_d+\mu_h+1\right)\Omega_d^2\right)(\alpha+1)\,\Omega_v^2+\Omega_d^2\end{pmatrix}\\
\mu_w\left(\mu_d+\mu_h+\mu_w\right)\Omega_{1,2}^2\\
+\mu_w\Omega_d^2\Omega_v^2\left(\mu_d+\mu_h+\mu_w\right)(\alpha+1)
\end{pmatrix}^2\Omega_{1,2}^2
$$

(A.4)

$$
N_2=2\Omega\xi_v\begin{pmatrix}
\Omega^2\left(-\left(\mu_h+\mu_w\right)(\alpha+1)\,\Omega_v^2+\Omega^2\right)\mu_w\left(\sin^2(\theta)\right)\\
+\Omega^2\Omega_v^2\mu_d\mu_w(\alpha+1)\left(\cos^2(\theta)\right)\\
-(\alpha+1)\begin{pmatrix}\left(\mu_d^2+\left(\mu_h+2\mu_w+1\right)\mu_d+\mu_h+\mu_w\right)\Omega^2\\-\Omega_d^2\left(\mu_d+\mu_w+1\right)\left(\mu_d+\mu_h+\mu_w\right)\end{pmatrix}\Omega_v^2\\
+\Omega^2\left(\left(\mu_d+\mu_h\right)\Omega^2-\Omega_d^2\left(\mu_d+\mu_h+\mu_w\right)\right)
\end{pmatrix}
+\mathrm{i}\left(-\Omega_v\alpha\begin{pmatrix}
\Omega^2\mu_w\left(\left(-\mu_h-\mu_w\right)\Omega_v^2+\Omega^2\right)\left(\sin^2(\theta)\right)\\
+\left(\cos^2(\theta)\right)\Omega^2\Omega_v^2\mu_d\mu_w\\
+\begin{pmatrix}\left(-\mu_d^2+\left(-\mu_h-2\mu_w-1\right)\mu_d-\mu_h-\mu_w\right)\Omega^2\\+\Omega_d^2\left(\mu_d+\mu_w+1\right)\left(\mu_d+\mu_h+\mu_w\right)\\+\Omega^2\left(\left(\mu_d+\mu_h\right)\Omega^2-\Omega_d^2\left(\mu_d+\mu_h+\mu_w\right)\right)\end{pmatrix}\Omega_v^2
\end{pmatrix}\right)
$$

(A.5)

$$\Delta_v = 2\left\{\begin{array}{c} \Omega^4\Omega_v^2\mu_w\left(\mu_d+\mu_h\right)(\alpha+1)\left(\cos^2(\theta)\right) \\ +\left(\Omega^2-1-\mu_w(\alpha+1)\Omega_v^2\right)\Omega^4\mu_w\left(\sin^2(\theta)\right)+\left(\mu_d+\mu_h\right)\Omega^6 \\ +\left(\begin{array}{c}-(\alpha+1)\left(\left(2\mu_d+2\mu_h+1\right)\mu_w+\left(\mu_d+\mu_h+1\right)\left(\mu_d+\mu_h\right)\right)\Omega_v^2 \\ +\left(-\mu_d-\mu_h-\mu_w\right)\Omega_d^2-\mu_d-\mu_h\end{array}\right)\Omega^4 \\ +\left((\alpha+1)\left(1+\left(\mu_d+\mu_h+\mu_w+1\right)\Omega_d^2\right)\Omega_v^2+\Omega_d^2\right)\left(\mu_d+\mu_h+\mu_w\right)\Omega^2 \\ -\Omega_d^2\Omega_v^2\left(\mu_d+\mu_h+\mu_w\right)(\alpha+1)\end{array}\right\}\Omega\xi_v + \mathrm{i}\left\{-\Omega_v\alpha\left\{\begin{array}{c} \Omega^4\mu_w\left(-\Omega_v^2\mu_w+\Omega^2-1\right)\left(\sin^2(\theta)\right) \\ +\Omega^4\Omega_v^2\mu_w\left(\mu_d+\mu_h\right)\left(\cos^2(\theta)\right)+\left(\mu_d+\mu_h\right)\Omega^6 \\ +\left(\begin{array}{c}\left(\left(-2\mu_d-2\mu_h-1\right)\mu_w-\left(\mu_d+\mu_h+1\right)\left(\mu_d+\mu_h\right)\right)\Omega_v^2 \\ +\left(-\mu_d-\mu_h-\mu_w\right)\Omega_d^2-\mu_d-\mu_h\end{array}\right)\Omega^4 \\ +\left(\left(1+\left(\mu_d+\mu_h+\mu_w+1\right)\Omega_d^2\right)\Omega_v^2+\Omega_d^2\right)\left(\mu_d+\mu_h+\mu_w\right)\Omega^2 \\ -\Omega_d^2\Omega_v^2\left(\mu_d+\mu_h+\mu_w\right)\end{array}\right\}\right\} \tag{A.6}$$

Data availability

No data was used for the research described in the article.

References

[1] J.-C. Wu, M.-H. Shih, Y.-Y. Lin, Y.-C. Shen, Design guidelines for tuned liquid column damper for structures responding to wind, Eng. Struct. 27 (13) (2005) 1893–1905, http://dx.doi.org/10.1016/j.engstruct.2005.05.009.

[2] S. Colwell, B. Basu, Tuned liquid column dampers in offshore wind turbines for structural control, Eng. Struct. 31 (2) (2009) 358–368, http://dx.doi.org/10.1016/j.engstruct.2008.09.001.

[3] R. Debbarma, S. Chakraborty, S.K. Ghosh, Optimum design of tuned liquid column dampers under stochastic earthquake load considering uncertain bounded system parameters, Int. J. Mech. Sci. 52 (10) (2010) 1385–1393, http://dx.doi.org/10.1016/j.ijmecsci.2010.07.004.

[4] H.H. Lee, S.-H. Wong, R.-S. Lee, Response mitigation on the offshore floating platform system with tuned liquid column damper, Ocean Eng. 33 (8–9) (2006) 1118–1142, http://dx.doi.org/10.1016/j.oceaneng.2005.06.008.

[5] S. Chakraborty, R. Debbarma, Stochastic earthquake response control of structures by liquid column vibration absorber with uncertain bounded system parameters, Struct. Saf. 33 (2) (2011) 136–144, http://dx.doi.org/10.1016/j.strusafe.2011.01.001.

[6] Q. Wang, H. Qiao, D. De Domenico, Z. Zhu, Y. Tang, Seismic performance of optimal multi-tuned liquid column damper-inerter (MTLCDI) applied to adjacent high-rise buildings, Soil Dyn. Earthq. Eng. 143 (2021) 106653, http://dx.doi.org/10.1016/j.soildyn.2021.106653.

[7] B. Chen, Z. Zhang, X. Hua, Closed-form optimal calibration of a tuned liquid column damper (TLCD) for flexible structures, Int. J. Mech. Sci. 198 (2021) 106364, http://dx.doi.org/10.1016/j.ijmecsci.2021.106364.

[8] B. Chen, Z. Zhang, X. Hua, B. Basu, Optimal calibration of a tuned liquid column damper (TLCD) for rotating wind turbine blades, J. Sound Vib. 521 (2022) 116565, http://dx.doi.org/10.1016/j.jsv.2021.116565.

[9] M.-A. Xue, J. Yang, X. Yuan, Z. Lu, J. Zheng, P. Lin, Vibration controlling effect of tuned liquid column damper (TLCD) on support structural platform (SSP), Ocean Eng. 306 (2024) 118117, http://dx.doi.org/10.1016/j.oceaneng.2024.118117.

[10] C. Masnata, A. Di Matteo, C. Adam, A. Pirrotta, Efficient estimation of tuned liquid column damper inerter (TLCDI) parameters for seismic control of base-isolated structures, Computer- Aided Civ. Infrastruct. Eng. 38 (12) (2023) 1638–1656, http://dx.doi.org/10.1111/mice.12929.

[11] Q.H. Cao, Vibration control of structures by an upgraded tuned liquid column damper, J. Eng. Mech. 147 (9) (2021) 04021052, http://dx.doi.org/10.1061/(ASCE)EM.1943-7889.0001965.

[12] S. Chowdhury, R. Debbarma, Presenting the potential of optimum torsionally coupled base isolators for vibration control of torsionally coupled structures: Exact closed-form expressions, J. Struct. Des. Constr. Pr. 30 (2) (2025) 04024111, http://dx.doi.org/10.1061/JSDCCC.SCENG-1616.

[13] S. Chowdhury, S. Adhikari, Nonlinear inertial amplifier liquid column dampers, Appl. Math. Model. 140 (2025) 115875, http://dx.doi.org/10.1016/j.apm.2024.115875.

[14] C. Masnata, A. Di Matteo, C. Adam, A. Pirrotta, Nontraditional configuration of tuned liquid column damper inerter for base-isolated structures, Mech. Res. Commun. 129 (2023) 104101, http://dx.doi.org/10.1016/j.mechrescom.2023.104101.

[15] H. Ding, Y.-N. Chen, J.-T. Wang, O. Altay, Numerical analysis of passive toroidal tuned liquid column dampers for the vibration control of monopile wind turbines using FVM and FEM, Ocean Eng. 247 (2022) 110637, http://dx.doi.org/10.1016/j.oceaneng.2022.110637.

[16] H. Ding, W. Wang, J.-F. Liu, J.-T. Wang, Z.-J. Le, J. Zhang, G.-M. Yu, On the size effects of toroidal tuned liquid column dampers for mitigating wind-and wave-induced vibrations of monopile wind turbines, Ocean Eng. 273 (2023) 113988, http://dx.doi.org/10.1016/j.oceaneng.2023.113988.

[17] M.U. Shah, M. Usman, S.H. Farooq, M. Rizwan, Spring-controlled modified tuned liquid column ball damper for vibration mitigation of structures, J. Sound Vib. 545 (2023) 117443, http://dx.doi.org/10.1016/j.jsv.2022.117443.

[18] Z.J. del Prado, M.V. Morais, Y.L. Martins, S.M. Avila, Nonlinear analysis of a wind turbine tower with a tuned liquid column damper (TLCD), Arch. Appl. Mech. 94 (9) (2024) 2417–2430, http://dx.doi.org/10.1007/s00419-024-02645-y.

[19] H.Q. Cao, N.-A. Tran, H.-L. Bui, Hedge-algebras-based hybrid control of earthquake-induced buildings using upgraded tuned liquid column dampers, Soil Dyn. Earthq. Eng. 182 (2024) 108728, http://dx.doi.org/10.1016/j.soildyn.2024.108728.

[20] N.-A. Tran, H.-L. Bui, Q.-H. Cao, U-shaped and V-shaped tuned liquid column dampers in vibration reduction of earthquake-induced buildings: A comparative study, in: Structures, 65, Elsevier, 2024, 106669, http://dx.doi.org/10.1016/j.istruc.2024.106669.

[21] A. Batou, S. Adhikari, Optimal parameters of viscoelastic tuned-mass dampers, J. Sound Vib. 445 (2019) 17–28, http://dx.doi.org/10.1016/j.jsv.2019.01.010.

[22] S. Chowdhury, A. Banerjee, S. Adhikari, The optimum enhanced viscoelastic tuned mass dampers: Exact closed-form expressions, J. Vib. Control 30 (5–6) (2024) 1080–1102, http://dx.doi.org/10.1177/10775463231156240.

[23] A. Di Matteo, C. Masnata, C. Adam, A. Pirrotta, Optimal design of tuned liquid column damper inerter for vibration control, Mech. Syst. Signal Process. 167 (2022) 108553, http://dx.doi.org/10.1016/j.ymssp.2021.108553.

[24] Z. Zhao, R. Zhang, Y. Jiang, C. Pan, A tuned liquid inerter system for vibration control, Int. J. Mech. Sci. 164 (2019) 105171, http://dx.doi.org/10.1016/j.ijmecsci.2019.105171.

[25] P.G.M. Database, Near-field pulse-like earthquake records, 2021, https://peer.berkeley.edu/peer-strong-ground-motion-databasesAvailable from the PEER Ground Motion Database at https://peer.berkeley.edu/peer-strong-ground-motion-databases.